Scientia Pharmaceutica

ÖSTERREICHISCHE PHARMAZEUTISCHE GESELLSCHAFT

MDPI

Article

Targeting PD-1/PD-L1-MAPK1 Signaling by a Novel Synergistic Combination of Rivastigmine and Epigallocatechin in Alzheimer's Disease: An Integrated In Silico Approach

Bhaswati Das and Marakanam Srinivasan Umashankar *

Department of Pharmaceutics, SRM College of Pharmacy, Faculty of Medicine and Health Sciences, SRM Institute of Science and Technology, Kattankulathur, Chengalpattu 603203, Tamil Nadu, India; bd5105@srmist.edu.in

* Correspondence: umashans@srmist.edu.in

Abstract

This study investigates the synergistic therapeutic potential of Rivastigmine (RVG) and Epigallocatechin (EGC) in Alzheimer's disease (AD), a multifactorial neurodegenerative disorder characterized by neuroinflammation, oxidative stress, and dysregulated signaling pathways. Conventional therapies primarily provide symptomatic relief and target limited pathways, highlighting the need for multi-target strategies with improved efficacy and safety. An integrated in silico approach combining pharmacokinetic evaluation, network pharmacology, molecular docking, and molecular dynamics simulations is used to determine the synergistic potential of RVG and EGC. Pharmacokinetic analysis indicates favorable drug-likeness and acceptable ADME/Tox profiles for both compounds. Network pharmacology identified 146 overlapping targets associated with AD, highlighting key hub genes including *NFKB1*, *MAPK1*, *STAT1*, *PRKACA*, *GRB2*, *LYN*, and *PTPN11*, which are involved in neuroinflammation, synaptic signaling, and neuronal survival. Functional enrichment analysis indicated significant involvement of MAPK/ERK signaling and immune-regulatory pathways. Importantly, the PD-1/PD-L1 signaling pathway is identified as a novel mechanism connecting neuroimmune modulation with intracellular kinase-driven neurodegeneration. Molecular docking studies showed strong binding affinities of RVG and EGC toward key AD-related targets, particularly *MAPK1*, supported by stable hydrogen bonding and interaction profiles. Molecular dynamics simulations confirmed stable protein-ligand interactions, with EGC contributing structural stability and RVG exhibiting adaptive flexibility within the binding pocket. These results suggest that the RVG-EGC combination exhibits synergistic potential by simultaneously modulating neuroinflammatory, oxidative stress, and kinase-mediated signaling pathways. The integration of PD-1/PD-L1 and MAPK/ERK signaling provides a novel mechanistic pathway for multi-target therapeutic intervention in AD.

Keywords: rivastigmine; epigallocatechin; MAPK/ERK signaling; PD-1/PD-L1; synergistic therapy; neuroinflammation

Academic Editors: Osvaldo Andrade Santos-Filho and Arthur Eugen Kümmerle

Received: 21 May 2026
Revised: 26 June 2026
Accepted: 1 July 2026
Published: 10 July 2026

1. Introduction

Neurodegenerative disorders are characterized by progressive loss of neuronal structure and function, leading to cognitive and motor impairments. Among these, Alzheimer's disease (AD) and Parkinson's disease (PD) represent the most clinically significant conditions, with AD primarily affecting cognition and memory, while PD largely impairs motor

function. These disorders play a significant role in clinical, social, and economic burden, as their chronic and irreversible progression leads to loss of independence, increased caregiver dependency, and substantial healthcare costs [1,2]. The growing aging population further increases this burden, making neurodegenerative diseases a major global public health challenge. According to the epidemiological perspective, AD is the leading cause of dementia, accounting for approximately 60–80% of cases worldwide, with nearly 50 million individuals currently affected and projections reaching 139 million by 2050 [3]. PD affects around 6 million people globally, with incidence expected to rise steadily. Beyond prevalence, the impact of these diseases extends to reduced quality of life, long-term institutional care, and significant emotional and financial strain on families and healthcare systems [4].

Patho-physiologically, AD is characterized by β-amyloid plaque deposition, tau neurofibrillary tangles, synaptic dysfunction, and progressive neuronal loss. In addition to these classical markers, mitochondrial dysfunction has emerged as a significant contributor, resulting in impaired ATP production and elevated oxidative stress [5]. Disruptions in neuronal plasticity and extracellular matrix homeostasis further limit the brain's ability to repair and adapt, thereby accelerating cognitive decline and disease progression. These multifactorial mechanisms highlight the complexity of AD and the limitations of single-target therapeutic strategies [6]. Current pharmacological management primarily involves cholinesterase inhibitors such as Rivastigmine (RVG), Donepezil, and Galantamine, along with the NMDA receptor antagonist Memantine. Although these agents provide moderate symptomatic relief, they do not reverse disease progression. Moreover, their prolonged use is frequently associated with adverse effects, including gastrointestinal disturbances, bradycardia, and sleep-related disorders, limiting patient compliance and therapeutic effectiveness. These limitations highlight a significant need for improved therapeutic strategies that can address both symptoms and underlying disease mechanisms [7].

Recent advancements introduced biologics such as Lecanemab and Donanemab, indicating the ability to slow cognitive and functional decline. However, limitations regarding safety, cost, and variable efficacy have led to mixed responses within the scientific community. Simultaneously, progress in biomarker development, including PET imaging, cerebrospinal fluid analysis, and blood-based assays improved diagnostic accuracy and enabled earlier intervention. In this context, growing attention is directed toward integrating naturally derived bioactive compounds with established therapeutics [8,9]. Epigallocatechin (EGC), a catechin, exhibits potent antioxidant, anti-inflammatory, and anti-amyloidogenic properties, along with the ability to modulate mitochondrial dysfunction and support neuronal survival. The rationale for combining EGC with RVG agents shows their complementary and multi-targeted mechanisms of action (Figure 1). While Rivastigmine primarily addresses neurotransmitter deficits associated with cognitive decline through enhancement of cholinergic signaling, EGC targets upstream pathological processes, including oxidative stress, mitochondrial dysfunction, and β-amyloid aggregation. This integrative approach enables simultaneous modulation of both symptomatic pathways and highlights disease-driving mechanisms. Such a combination strategy is a promising approach in Alzheimer's disease, where single-target therapies often fail to address the complex and interconnected network of pathological events. By concurrently targeting cholinergic dysfunction, oxidative damage, mitochondrial impairment, and amyloid pathology, the combined use of RVG and EGC provides a more potent therapeutic approach [10]. This synergy not only supports improved cognitive function but also offers the potential to attenuate disease progression by modulating at multiple stages of the pathological cascade. Therefore, the integration of RVG with EGC represents a promising and rational strategy for enhancing therapeutic efficacy and advancing the overall management of Alzheimer's disease.

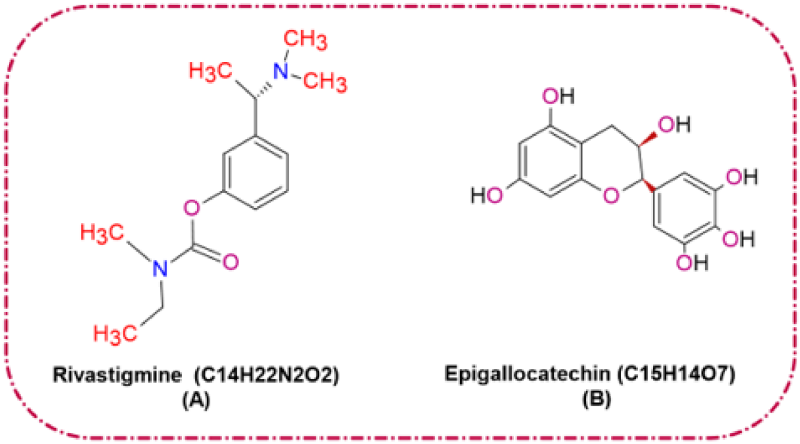

Figure 1. Chemical structures of (**A**) Rivastigmine ($C_{14}H_{22}N_2O_2$) and (**B**) Epigallocatechin ($C_{15}H_{14}O_7$), illustrating their key functional groups and structural features relevant to their pharmacological activity in Alzheimer's disease.

In the present study, an integrated in silico and experimental strategy to evaluate the pharmacological and synergistic efficacy of the selected agents. Although RVG and EGC individually show neuroprotective and anti-inflammatory activities, their combined therapeutic interactions and the molecular mechanisms highlighting their synergistic effects remain insufficiently explored. Previous studies have shown that MAPK/ERK signaling regulates PD-L1 expression in several cancer models, indicating a well-reported interaction between intracellular kinase signaling and immune checkpoint regulation. Emerging evidence also indicates that both MAPK/ERK signaling and the PD-1/PD-L1 (Programmed Cell Death Protein 1/Programmed Death-Ligand 1) signaling contribute to neuroinflammation and AD pathogenesis. Based upon these observations, the present study aimed to evaluate the synergistic potential of RVG and EGC and to investigate their integrated target network, with particular emphasis on the potential involvement of the PD-1/PD-L1–MAPK1 signaling in AD [11,12]. SwissADME and pkCSM analyses, network pharmacology, protein–protein interaction analysis, molecular docking, molecular dynamics simulations, and Chou–Talalay combination analysis were subsequently performed to characterize pharmacokinetic properties, identify potential therapeutic targets, and evaluate molecular interactions and synergistic dose combinations.

2. Methodology

2.1. In Silico Drug Likeness and ADMET Analysis

The pharmacokinetic profile and toxicity properties of RVG and EGC are assessed by the online tools pkCSM (http://biosig.unimelb.edu.au/pkcsm/, accessed 1 February 2026) and SWISS-ADME (https://www.swissadme.ch/, accessed 1st February 2026), which are widely used for predicting drug-likeness, ADME properties, and safety profiles. SWISS-ADME is used to validate the estimated key parameters related to absorption, metabolism, and distribution, along with physicochemical characteristics, whereas pkCSM integrates information from both in vivo and in vitro studies to predict significant toxicity risks with an overall safety profile. Drug-likeness is assessed by Lipinski's Rule of Five, and its parameters include molecular weight $\leq$ 500 Da (MW), hydrogen bond donors $\leq$ 5 (HBD), LogP $\leq$ 5, and hydrogen bond acceptors $\leq$ 10 (HBA). Pharmacokinetic predictions, such as intestinal absorption, with values $\geq$ 30% regarded as acceptable, and Blood–Brain Barrier permeability expressed as logBB. Toxicological assessment involved prediction of hERG I inhibition, where non-inhibition suggests reduced cardiotoxic risk; acute oral toxicity in rats represented as an LD50 mg/kg range exceeding 300 mg/kg, indicating potential

hepatotoxicity. These parameters help in a comprehensive evaluation of the ADMET profile of RVG and EGC, supporting their suitability in terms of pharmacokinetics and safety [11].

2.2. Pharmacological Network Analysis

2.2.1. Mapping the Disease-Associated Gene and Target Prediction

SMILES formats for RVG and EGC were obtained from PubChem and subsequently uploaded to the SuperPred web server for computational prediction of the target (https://prediction.charite.de, accessed on 15 February 2026). To investigate disease-associated genes, the determined targets of compounds (RVG and EGC) were compared with a dataset of genes associated with Alzheimer's disease, retrieved from the GeneCards database using the keyword "Alzheimer's disease" (https://www.genecards.org, accessed on 15 February 2026). Common targets shared between the predicted compounds and disease-associated genes were identified through overlap analysis and further represented using Venny tools (https://www.interactivenn.net/, accessed on 15 February 2026). However, this approach enabled the identification of significant molecular targets and provided insights into the therapeutic mechanisms of RVG and EGC in Alzheimer's disease [12,13].

2.2.2. Identification of Shared RVG-EGC Targets in AD

Common targets predicted from the Venny analysis were integrated; duplicate entries were deleted to ensure data reliability. PPI analysis was performed using the STRING online tool (https://string-db.org/, accessed on 20 February 2026), with the organism chosen as *Homo sapiens*, applying a high-confidence score threshold of 0.700 while excluding unconnected nodes. The generated interaction data was downloaded in TSV format and further imported into Cytoscape (v3.9.1) for representation; the nodes indicate edges, and proteins indicate their interaction profiles. Key genes within the networks are identified by the CytoHubba plugin (v0.1) based on centrality of degree, enabling the prediction of highly interconnected and potentially significant molecular targets involved in AD [14,15].

2.2.3. Analysis of Functional Modules

To detect highly interconnected nodes within the PPI network, clustering analysis is analyzed by MCODE (v2.0.3) plugin in Cytoscape. The earlier established PPI network of common targets associated with RVG and EGC in AD is used as the input dataset. The analysis is conducted using standard parameters, including node score cutoff = 0.2, degree cutoff = 2, maximum depth = 100, and k-core = 2. The resulting clusters are arranged based on their scores, and the most significant clusters with higher scores are selected for further analysis. Each identified cluster was evaluated in terms of node and edge distribution, and its biological relevance is interpreted based on the gene composition within each cluster. This approach facilitated the identification of significant molecular networks and functional components that may play a significant role in the progression and pathology of AD [16].

2.2.4. Analysis of Compound-Target-Pathway (CTP) Interactions

The CTP network is used to observe the interactions between RVG and EGC, their predicted molecular targets, and the associated pathways in AD. The top 10 hub genes identified through Cytohubba (v0.1) analysis were chosen for pathway enrichment analysis using (https://www.kegg.jp, accessed 25 February 2026) the KEGG-database, facilitated by the (https://david.ncifcrf.gov/, accessed 25 February 2026) DAVID bioinformatics platform. Potentially enriched pathways ($p < 0.05$) were identified and aligned with their respective target genes. However, the integrated data CTP-gene-disease relationships were opened into Cytoscape Version 3.9.1 for network construction and visualization. This network highlights the multi-target and pathway interactions of these selected compounds,

providing insights into their potential roles in regulating key signaling pathways associated with the pathogenesis of AD [17,18].

2.2.5. Functional Enrichment (GO) and KEGG Pathway Analysis

Functional analysis is carried out by the DAVID bioinformatics platform to explore the physiological significance of targets associated with RVG and EGC in AD. The overlapping target genes are applied to Kyoto Encyclopedia of Genes and Genomes (KEGG) Pathway Analysis and Gene Ontology (GO) Enrichment Analysis, with the organism specified as *Homo sapiens*. GO annotations are classified into three: Biological Process (BP), Cellular Component (CC), and Molecular Function (MF). GO and enriched pathway terms are chosen based on statistical significance criteria of $p < 0.05$ and further prioritized according to gene count relevance. Enrichment results are represented using bar charts and bubble plots generated through the SR-plot online platform (https://www.bioinformatics.com.cn/en, accessed on 1 March 2026). Prior to analysis, repeated targets are eliminated to ensure data accuracy and consistency throughout the enrichment process [19,20].

2.3. Molecular Docking Study

Docking studies for RVG and EGC for the predicted targets are performed using the *Schrödinger-Suite version 2023-1*. The three-dimensional analysis of targets is taken from the RCSB Protein Data Bank (https://www.rcsb.org/, accessed on 10 March 2026) and the PDB IDs are 8TQD, 1TVO, 1YVL, 2GU8, and 7MPH. Protein preparations are performed using the Protein Preparation Wizard, which helps to remove crystallographic water molecules, add side chains and missing residues, and restrain minimization by the OPLS4 Force Field with an atom RMSD cutoff of 0.30 Å. To assess the validity of the docking protocol, ligands co-crystallized with the protein structures are used as reference molecules, and docking is performed using the same grid parameters. Ligand preparation for RVG and EGC is conducted using the LigPrep module, and the ionization states were generated using Epik under physiological pH conditions (7.0 ± 2.0). The ligands are further minimized with OPLS4, and the minimum-energy conformations are selected for molecular docking analysis. Receptor grids are formed by Grid Generation module by center the grid box on the active position of every protein: *NFkB1* (x = 7.31, y = −14.33, z = −13.31), 1TVO (x = 6.42, y = −4.37, z = 16.44), 2GU8 (x = −9.29, y = −10.58, z = 2.21), 1YVL (x = −23.32, y = −1.96, z = 104.33), and 7MPH (x = 9.16, y = 12.17, z = 14.87). Docking is performed by a van der Waals factor of 1.0 and a partial charge cutoff range of 0.25. The Glide XP (extra precision) module is utilized for simulations, and the significant binding poses are further evaluated with the XP Visualizer to predict the important amino acid interactions modulating binding affinity. Furthermore, intermolecular interactions, including bond lengths and distances between ligands and target proteins, were evaluated using BIOVIA Discovery Studicato 2024. Docking scores kcal/mol and their interacting residues are recorded for further analysis of binding stability and interaction profiles [21,22].

2.4. Computational Molecular Dynamics (MD) Analysis

MD simulations of the top-ranked protein-ligand complexes are carried out by Desmond integrated with *Schrödinger Suite version 2023-1*. The final docking RVG and EGC complexes, taken from Glide XP precision, were selected for further dynamic study. Every complex is integrated into an orthorhombic box with a buffer distance of 10 Å and also solvated by the water model TIP3P. To maintain system neutrality, appropriate counterions were added, along with 0.15 M NaCl used to simulate a physiological ionic environment. This is subsequently subjected to equilibration and energy minimization by default relaxation protocol under the OPLS4 force field. The production run is performed for 100 ns with NPT ensemble conditions, such as regulating a constant temperature (CT) of 300 K

and the pressure of 1 atm by the Martyna–Tobias–Klein barostat. Post-simulation trajectory analyses, such as root-mean-square fluctuation (RMSF), root-mean-square deviation (RMSD), and interactions with hydrogen bonds, are used to assess structural integrity, flexibility, and dynamic behavior of the protein-ligand complexes [23,24].

2.4.1. Cell Culture

Human neuroblastoma SH-SY5Y cells (procured from NCCS, Pune, India) were cultured in Dulbecco's Modified Eagle Medium (DMEM) supplemented with 10% fetal bovine serum (FBS), L-glutamine, sodium bicarbonate, and antibiotics (penicillin, streptomycin, and amphotericin B), and maintained at 37 °C in a humidified atmosphere containing 5% CO_2. Cells were seeded at a density of 5×10^3 cells/well in 96-well plates and allowed to attach for 24 h. Subsequently, cells were treated with increasing concentrations of RVG and EGC individually and in fixed-ratio combinations (1:1, 1:2, and 2:1). Following 48 h of incubation, cell viability was assessed using the MTT (3-(4,5-Dimethylthiazol-2-yl)-2,5-diphenyltetrazolium Bromide) assay, and absorbance was measured at 540 nm. All experiments were performed in triplicate, including untreated control wells [25–27].

2.4.2. Chou-Talalay Analysis

Pharmacodynamic interactions between RVG and EGC were evaluated using the Chou-Talalay method implemented in CompuSyn software Version 1.0 (Paramus, NJ, USA). Fixed-ratio combinations (1:1, 1:2, and 2:1) were analyzed using cell viability data obtained from the MTT assay to generate dose-effect curves based on the median-effect principle. Combination index (CI), fraction affected (Fa), dose reduction index (DRI), and isobologram analyses were performed to quantitatively characterize the interactions between the two compounds. According to the Chou-Talalay criteria, CI values < 1, =1, and >1 indicate synergistic, additive, and antagonistic effects, respectively, while DRI values > 1 reflect favorable dose reduction in combination therapy. These analyses facilitated the identification of the optimal RVG:EGC combinations for subsequent studies [28,29].

3. Results

3.1. Pharmacokinetic and Physicochemical Characteristic Study

The pharmacokinetic and toxicity characteristics of RVG and EGC were assessed by computational prediction tools to evaluate their suitability as potential therapeutic agents for AD. Both compounds showed overall favorable pharmacokinetic characteristics and acceptable safety profiles. Based on physicochemical property analysis, RVG adhered to Lipinski's drug-likeness criteria, while EPI showed a single violation related to hydrogen bond donors (NH or OH > 5) (Table 1).

Table 1. Drug-likeness properties of RVG and EGC.

Compounds Name	Molecular Weight (MW)	Hydrogen Bond Acceptor (HBA)	Hydrogen Bond Donor (HBD)	Lipophilicity (LogP)	Lipinski Rule	No. of Rotatable Bonds	Topological Polar Surface Area (TPSA)
RVG	250.17	3	0	1.86	0	4	25.09
EGC	306.07	7	6	0.26	1	1	105.93

RVG exhibited higher intestinal absorption (88.456%) compared to EPI (54.128%), suggesting more efficient gastrointestinal absorption. Compared to blood–brain barrier (BBB) permeability, RVG showed a positive logBB value (0.508), indicating greater BBB penetration, whereas EPI exhibited low BBB (−1.377). Similarly, central nervous system (CNS) permeability predictions indicated limited CNS penetration for both compounds,

with RVG (−2.255) showing relatively higher permeability than EGC (−3.507), suggesting a lower level of CNS-related toxicity, particularly for EPI. Neither RVG nor EGC is predicted to inhibit the hERG I channel, indicating a lower risk of cardiotoxicity. RVG and EGC are non-hepatotoxic and non-sensitizing, enhancing their potential for prolonged therapeutic adherence. Acute toxicity following oral analysis revealed an LD_{50} range of 3.402 mol/kg for RIV and 2.492 mol/kg for EPI, both exceeding the threshold for low toxicity and indicating acceptable tolerability. Furthermore, chronic toxicity assessment showed a lower LOAEL for RIV (1.163 log mg/kg bw/day) than for EPI (2.927 log mg/kg bw/day), indicating improved safety for long-term administration (Table 2).

Table 2. Computationally derived ADME and safety parameters of RIV and EPI.

ADME/Toxicity Property	Reference Criterion for Favourability	RIV	EPI
Intestinal absorption (%)	>30% considered good absorption	88.456%	54.128%
Skin sensitization	Absence indicates safety	No	No
Blood–brain barrier permeability (BBB)	>0.3 indicates strong BBB	0.508	−1.377
CNS permeability (log BB)	log BB > −1 shows CNS penetration	−2.255	−3.507
hERG I channel inhibition	Absence suggests safety	No	No
Acute oral toxicity (LD50 mol/kg)	>1 suggests low toxicity	3.402	2.492
Chronic oral toxicity (LOAEL log mg/kg bw/day)	<2 indicates reduced chronic toxicity	1.163	2.927
Liver Toxicity	Absence indicates hepatosafety	No	No

3.2. Network-Based Pharmacological Analysis

3.2.1. Computational Target Identification and AD Association

Significant molecular targets of RVG and EGC are predicted by the SuperPRED online tool using their respective SMILES structures taken from the database of PubChem. The identified targets are subsequently analyzed by the STRING online database to identify PPI and pathway relations, leading to 86 targets for RVG and 111 targets for EGC being predicted. To identify disease-associated genes, a comprehensive set of 17,508 genes related to AD is obtained from the GeneCards online database by searching the keyword "Alzheimer's disease". These genes are reported to maintain key molecular signaling involved in the onset and disease progression of AD. The intersecting genes between AD-associated targets and the identified targets of RVG and EGC suggest their mechanistic involvement and therapeutic potential in AD.

3.2.2. Construction of the Target Interaction Network of RVG and EGC in AD

Interactive network analysis is used to identify common targets between AD-associated genes and the predicted molecular targets of RVG and EGC. A total of 84 common genes were identified for RVG, and 111 overlapping genes for EGC were obtained following comparison with AD-associated genes retrieved from the GeneCards online database (Figure 2A). After integration of the two datasets and removal of duplicate targets, a combined interaction network consisting of 146 nodes with 611 edges was constructed and shown in Cytoscape v3.8.0, providing a comprehensive overview of the shared molecular landscape regulated by RVG and EGC. To analyze key components within the network, Cytohubba was used to score the nodes by degree centrality. The analysis highlighted the top hub genes: *NFKB1*, *MAPK1*, *STAT1*, *PRKACA*, *GRB2*, *LYN*, *PTPN11*, *BRAF*, *CDK2*, and *CDK1* (Figure 2B; Table 3). These 10 hub genes play a significant regulatory role in critical biological processes associated with AD, including neuroinflammation, synaptic signaling, neuronal survival, and cell cycle regulation. *NFKB1* and *STAT1* play pivotal roles in inflammatory and immune-mediated signaling pathways

in neurodegeneration. *MAPK1*, *BRAF*, and *PRKACA* are key regulators of intracellular signaling cascades that influence neuronal plasticity and stress responses. *GRB2*, *LYN*, and *PTPN11* are involved in receptor-mediated signal transduction is essential for synaptic function and neuronal communication. *CDK1* and *CDK2* are associated with aberrant cell cycle re-entry, a phenomenon linked to neuronal loss in AD.

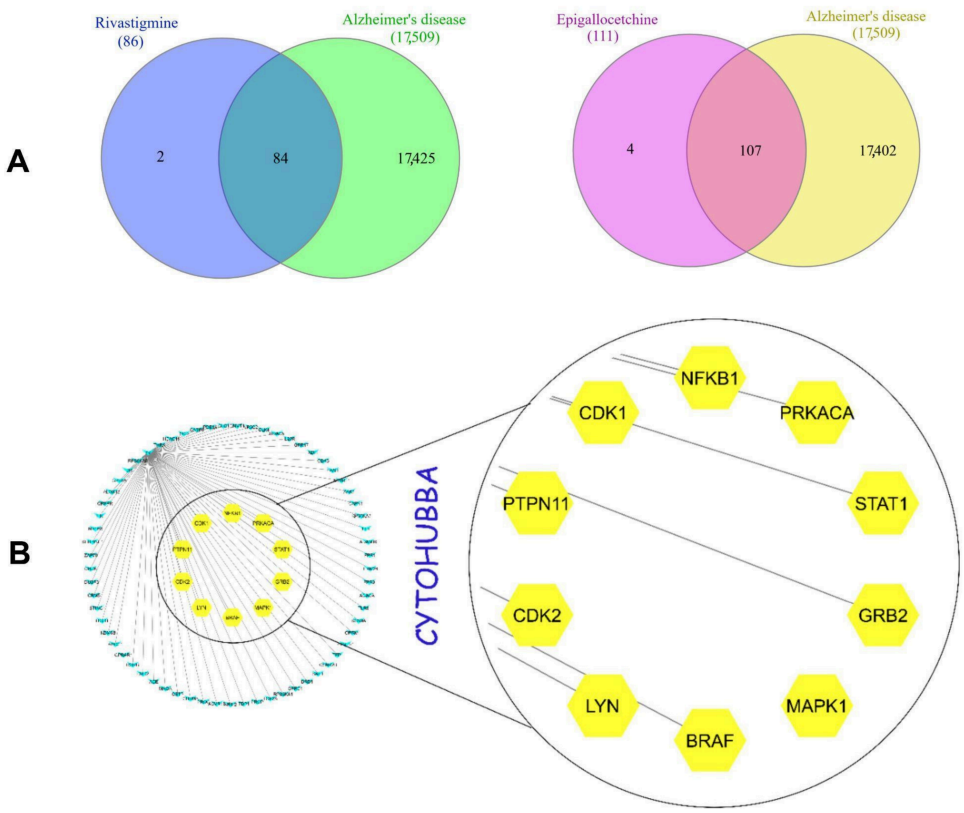

Figure 2. Network-based pharmacology prediction of RVG and EGC targets in AD. (**A**) shows Venn diagrams and the overlap between predicted targets of RVG and EPG with AD-associated genes, highlighting the common targets considered for further analysis. (**B**) A PPI network constructed from the overlapping targets using Cytoscape, and the nodes indicate proteins and the edges indicate their functional connectivity. Identification of hub genes using Cytohubba, with highlighted nodes representing the top-ranked genes (*CDK2*, *PTPN11*, *CDK1*, *NFKB1*, *PRKACA*, *STAT1*, *GRB2*, *MAPK1*, *BRAF*, and *LYN*) based on their degree of connectivity, suggesting their potential regulatory roles in Alzheimer's disease.

Table 3. Hub genes and their scores.

Gene	Code
NFKB1	40
MAPK1	31
STAT1	28
PRKACA	24
GRB2	24
LYN	23
PTPN11	22
BRAF	22
CDK2	21
CDK1	21

3.2.3. MCODE-Based Cluster Analysis

Clustering of common target proteins is performed by the MCODE in Cytoscape version 3.9.1 to determine the highly connected regions in the PPI network, representing biologically related functional modules. This analysis revealed six separate clusters exhibiting different connectivity levels, indicating that RVG and EGC may influence multiple biological processes involved in AD (Figure 3). Cluster 1 is a potential module, containing 11-nodes and 50-edges, and signaling molecules including *NFKB1*, *STAT1*, *MAPK1*, *BRAF*, *GRB2*, *LYN*, and *PTPN11*. This highly interconnected cluster represents a central signaling network associated with neuroinflammation, immune activation, and intracellular kinase signaling, which are critically involved in AD pathogenesis. Cluster 2 consisted of 20 nodes and 42 edges and included receptors and regulatory proteins involved in neuroimmune communication, neurotransmission, and oxidative stress responses. Cluster 3, containing five nodes and eight edges, is associated with cell cycle regulation and DNA-related processes. Aberrant activation of cell cycle-related pathways in post-mitotic neurons is a recognized contributor to neuronal loss in AD, indicating the potential relevance of this module to disease progression. Cluster 4 comprised three nodes and three edges, representing a compact epigenetic regulatory module involved in chromatin remodeling and transcriptional control. Dysregulation of epigenetic mechanisms is linked to impaired synaptic plasticity and memory deficits in AD. Cluster 5, also containing three nodes and three edges, is associated with vascular and proteolytic regulation that may influence cerebral perfusion, BBB integrity, and amyloid clearance mechanisms in AD. Cluster 6 included 9 nodes and 11 edges and involved genes related to oxidative stress defense, neurotransmitter transport, and calcium signaling, all important for maintaining neuronal homeostasis and preventing neurodegenerative damage.

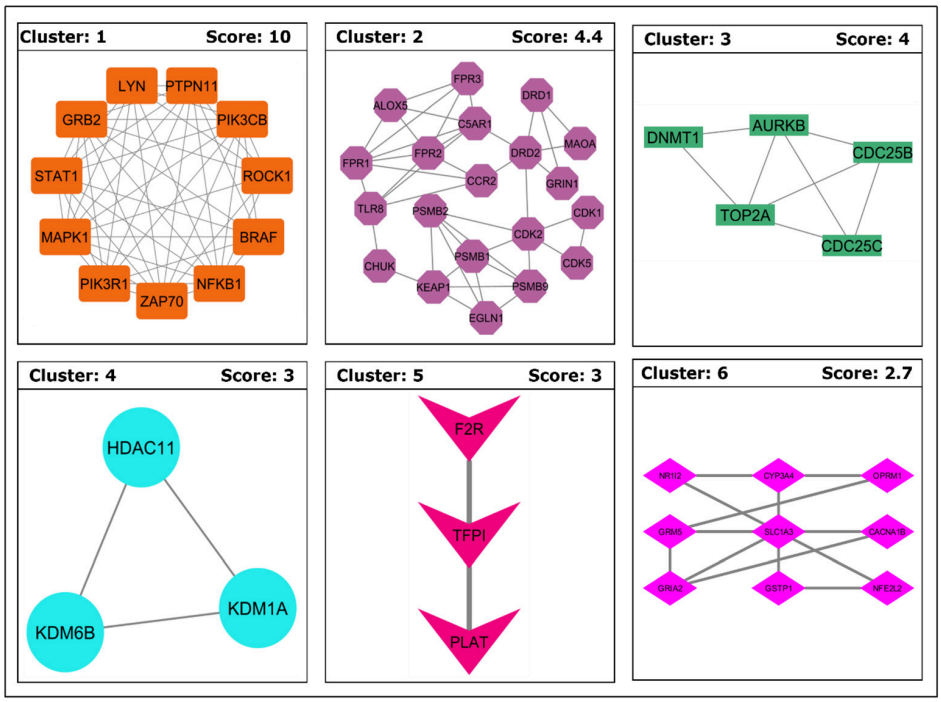

Figure 3. MCODE-based clustering of the RVG-EGC PPI network. Six functional clusters (Clusters 1–6) are extracted from the PPI network by the MCODE in Cytoscape, based on topological connectivity. Nodes represent proteins, while edges denote validated protein–protein interactions. Different node colors indicate individual protein members within each module. Cluster 1 (score: 10) represents the principal seed module and includes key hub proteins such as *MAPK1*, *STAT1*, and *GRB2*. The remaining clusters (Clusters 2–6) correspond to supporting functional modules associated with processes such as drug transport (e.g., *ABCC1*, *SLC19A1*) and metabolic regulation.

3.2.4. Analysis of Compound–Target Interactions

A CTPD network is constructed to represent the computational-level interactions of RVG and EGC in AD (Figure 4). The network integrates the relationships among the two compounds, their predicted molecular targets, associated signaling pathways, and AD, providing a comprehensive overview of their multi-target therapeutic potential. In the network, RVG and EGC occupy central positions and are extensively connected to multiple target genes and biological pathways implicated in AD pathogenesis. Several hub targets, including *NFKB1*, *STAT1*, *MAPK1*, *BRAF*, *GRB2*, *PRKACA*, *LYN*, *PTPN11*, *CDK1*, and *CDK2*, exhibit high connectivity within the network, highlighting their critical regulatory roles. These targets play a major role in neuroinflammation, immune signaling, synaptic function, cell cycle dysregulation, and neuronal survival in the development and progression of AD. The strong interconnections among these targets and multiple signaling pathways suggest that RVG and EGC alter AD-related mechanisms through coordinated regulation of interconnected molecular networks rather than single-target effects. Compared to the PPI network and MCODE analyses, this helps to predict the PPI and localized clusters. The CTPD network provides a comprehensive pathway-level perspective, linking molecular targets linked to higher-level biological processes and disease mechanisms.

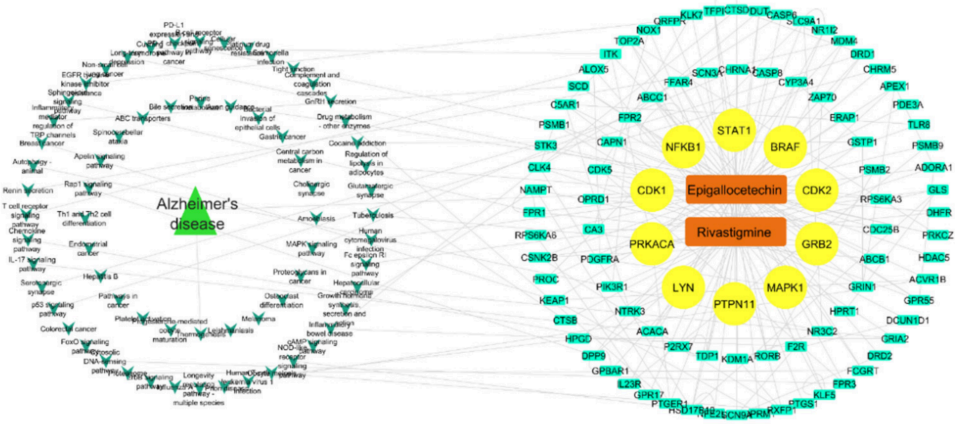

Figure 4. Compound-Target-Pathway (CTP) network of RVG and EGC in AD. The network shows the interactions between RVG and EGC (yellow diamond nodes), their predicted target proteins (blue rectangular nodes), and key hub genes (pink circular nodes), along with enriched signaling pathways (purple triangular nodes). The central orange node represents AD. Edges indicate the relationships between compounds, targets, and pathways, indicating a multi-target and multi-pathway regulatory framework. The highlighted hub genes (e.g., *STAT1*, *MAPK1*, *NFKB1*, *PRKACA*, *GRB2*, *CDK1*, *CDK2*, *BRAF*, *LYN*, and *PTPN11*) suggest their critical involvement in disease-associated signaling pathways, emphasizing the potential synergistic action of RVG and EGC in modulating AD pathophysiology.

3.2.5. KEGG and GO Functional Enrichment Analysis in AD

Gene Ontology (GO) functional enrichment is to evaluate the functional mechanisms highlighting the therapeutic potential of EGC and RVG in AD (Figure 5A). Enriched GO categories were organized into BP, CC, and MF classifications. In the BP category, significant enrichment is observed in signal transduction, protein phosphorylation, MAPK cascade, ERK1/ERK2 signaling, and DNA damage response, indicating that the therapeutic potential is primarily driven by regulation of intracellular pathways and stress-response mechanisms. These biological processes are closely related to significant pathological characteristics of AD, such as tau hyperphosphorylation, amyloid-beta-induced toxicity, and progressive neuronal degeneration. In the CC category, enriched terms such as cytosol, nucleus, nucleoplasm, mitochondrion, and centrosome indicate that the target proteins are distributed across significant subcellular compartments involved in transcriptional regulation, intracellular signaling, and energy metabolism. The enrichment of mitochon-

drial components further highlights the significant role of mitochondrial dysfunction and redox balance in the progression of neurodegeneration. In the MF category, strong enrichment is observed for protein kinase activity, cyclin-dependent kinase activity, protein serine/threonine kinase activity, ATP binding, and phosphotyrosine residue binding, indicating that dysregulated kinase-mediated phosphorylation is a key mediator of pathological signaling, particularly contributing to tau hyperphosphorylation and neuronal dysfunction in Alzheimer's disease.

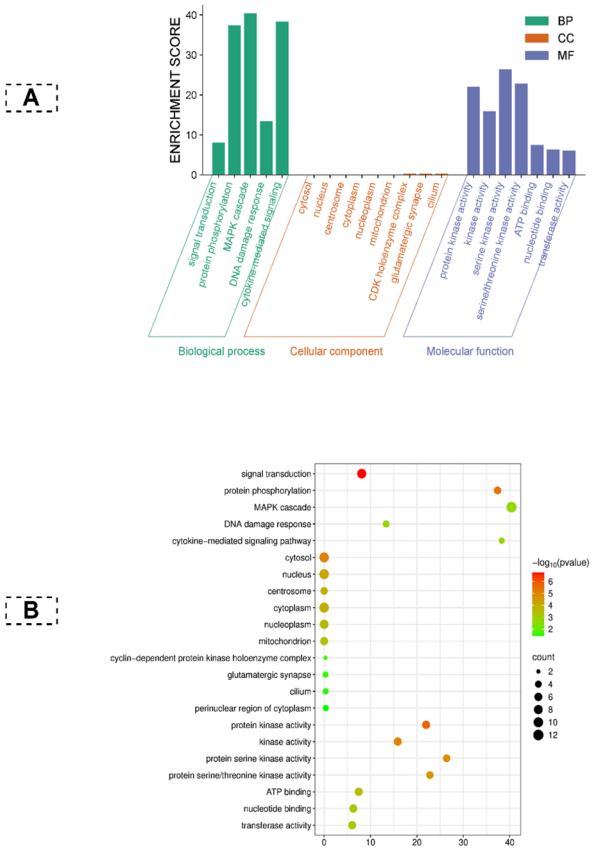

Figure 5. Functional enrichment analysis of RVG and EGC associated with AD. (**A**) GO enrichment analysis showing the key enriched terms under Biological Process (green), Cellular Component (orange), and Molecular Function (blue). Bar lengths correspond to the enrichment magnitude of each term. (**B**) Bubble plot representing significantly enriched GO categories; bubble size corresponds to the number of associated genes, and color gradient represents statistical significance based on −log10 (*p*-value), with darker shades indicating stronger significance.

KEGG enrichment functional analysis is used to determine the significant pathways related to the identified targets (Figure 5B). The analysis showed significant enrichment of pathways related to MAPK signaling, neuroinflammatory responses, and cellular stress pathways, plays an important role as regulators of synaptic plasticity, neuronal survival, and apoptosis. Key hub genes, including *NFKB1*, *MAPK1*, *STAT1*, *PRKACA*, *GRB2*, *LYN*, *PTPN11*, *BRAF*, *CDK2*, and *CDK1*, showed strong network connectivity, suggesting their central roles in modulating oxidative stress, inflammatory signaling, and protein aggregation in Alzheimer's disease. However, the PD-1/PD-L1 signaling pathway (Figure 5) plays a significant role in neuroimmune regulation and neuroinflammation. This pathway highlights that upstream activation of receptor-mediated signaling cascades, including *EGFR* and cytokine receptors, triggers downstream PI3K/AKT and MAPK signaling pathways. Within this pathway, the MAPK signaling (RAS-RAF-MEK-ERK) is significantly involved, and ERK (*MAPK1*) regulates transcription factors such as AP-1 and NF-κB.

Among the significantly enriched KEGG pathways (Figure 6), the canonical PD-L1 expression and PD-1 checkpoint signaling pathway is identified. Although this pathway is annotated by KEGG as a cancer-associated signaling pathway, its enrichment in the present analysis is mainly driven by common intracellular signaling molecules, particularly *MAPK1*, that are involved in neuroimmune regulation. Therefore, the pathway is examined to show the potential involvement of *MAPK1*-mediated signaling in AD rather than to suggest a cancer-specific mechanism. Importantly, PD-1 and PD-L1 are not identified among the overlapping targets; however, several genes associated with the KEGG PD-1/PD-L1 signaling pathway are involved in its enrichment. Therefore, the observed association shows pathway-level enrichment rather than direct targeting of PD-1 or PD-L1.

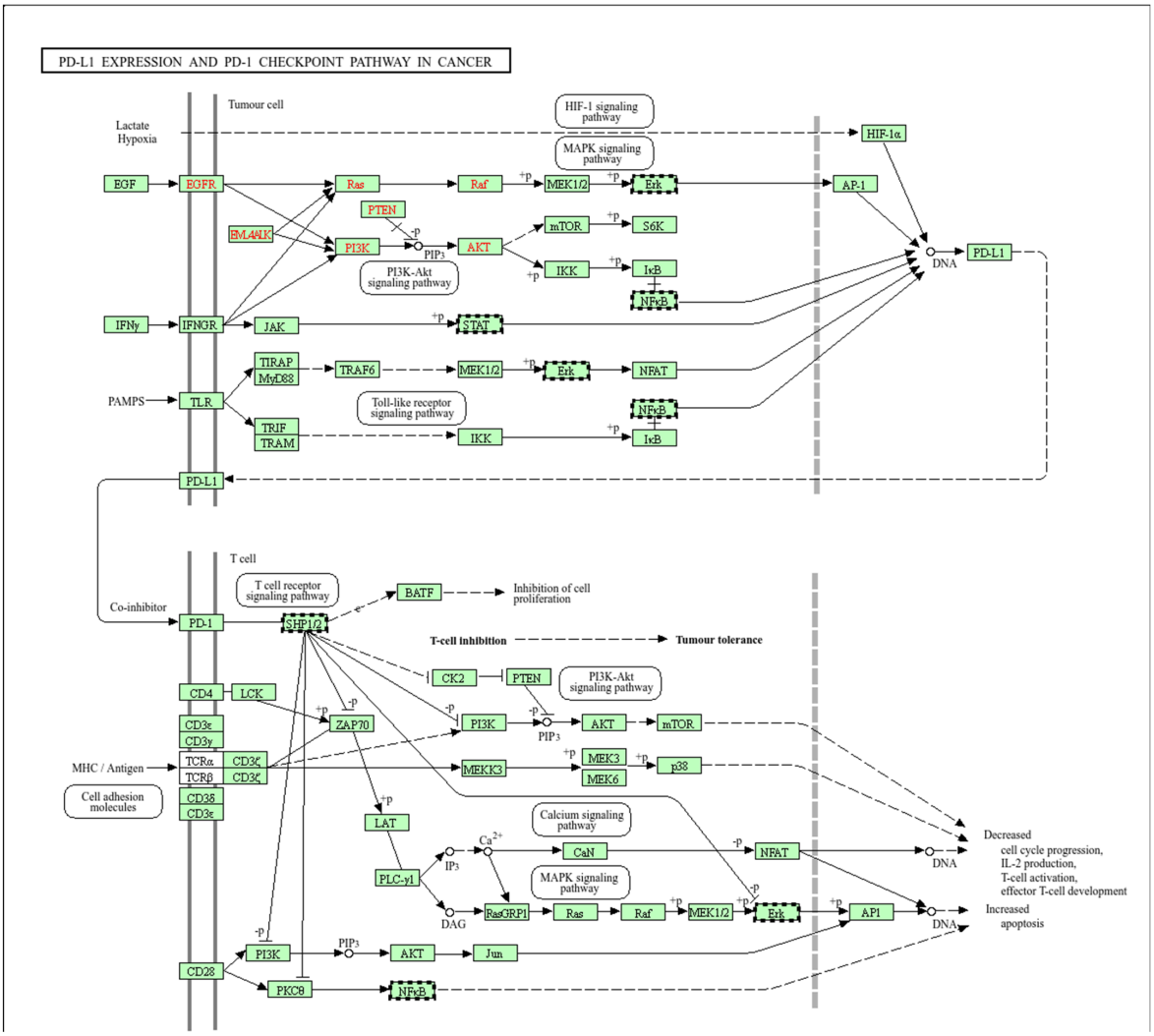

Figure 6. KEGG-derived PD-L1 expression and PD-1 checkpoint signaling pathway identified through DAVID enrichment analysis. Although this canonical pathway is annotated in KEGG as the PD-L1 expression and PD-1 checkpoint pathway in cancer, it is selected because it contains the enriched *MAPK1* signaling module identified in this network pharmacology analysis. The highlighted MAPK cascade shows the potential neuroimmune signaling explored in the present AD study rather than indicating a cancer-specific mechanism.

In Alzheimer's disease, aberrant activation of ERK is associated with increased tau phosphorylation, neuronal stress, and synaptic dysfunction. The PD-1/PD-L1 signaling pathway further modulates immune responses by influencing T-cell activity and inflammatory signaling, thereby contributing to chronic neuroinflammation observed in neurode-

generative conditions. Targeting ERK within this pathway suggests a potential therapeutic strategy, and modulation of MAPK signaling may attenuate downstream inflammatory responses, reduce abnormal phosphorylation events, and improve neuronal survival.

4. Docking-Based Interaction Analysis

The docking procedure is validated through redocking of the co-crystallized ligands of the selected target proteins, yielding an RMSD range below 2 Å (Table 4) supporting the validity and accuracy of the docking procedure. The top five hub proteins identified, *NFKB1*, *MAPK1*, *STAT1*, *PRKACA*, and *GRB2*, are subjected to MD with RVG and EGC to determine their binding affinities toward AD-associated targets. Docking scores presented in Table 5. varied between −8.63 and −3.49 kcal/mol, indicating differences in binding affinity among the selected targets. Among these, *MAPK1* exhibited the strongest interaction, with RVG showing the highest binding affinity (−8.63 kcal/mol), forming multiple interactions with residues such as *LYS164*, *ASP162*, *GLN132*, and *ARG135*. EGC also showed strong binding toward *MAPK1* (−7.32 kcal/mol), interacting with *ASP111*, *LYS151*, and *ASP167*. These interactions were further supported by conventional hydrogen bonds and their bond distances ranging from ~4.37 Å to 5.96 Å, indicating persistent ligand-protein interactions. Similarly, *NFKB1* showed significant binding, where RVG (−7.94 kcal/mol) formed hydrogen bonds with LYS243 (~5.68 Å), while EGC (−6.79 kcal/mol) established multiple hydrogen bonds with GLU62, ARG56, and *ALA244*, and its interaction bond distances ranged from ~4.29 Å to 4.47 Å. In the case of *STAT1*, moderate binding affinities are observed, with EGC (−6.61 kcal/mol) exhibiting relatively stronger interactions than RVG (−5.28 kcal/mol), validated by hydrogen-bonding interactions with GLU618 and ALA630 (~4.08–4.42 Å), whereas RVG interacted with MET654 (~4.46–5.42 Å). For *PRKACA*, both compounds displayed moderate binding, where RVG (−4.81 kcal/mol) formed hydrogen bonds with GLU127 and LYS168 (~5.66–6.04 Å), and EGC (−4.61 kcal/mol) interacted with amino acids LYS168, ASP166, and GLU170, with its bond distances ranging from ~4.13 Å to 5.21 Å. *GRB2* showed relatively weaker binding interactions, where RVG showed a docking score of −3.74 kcal/mol and formed a hydrogen bond with ASP94 at an approximate distance of 4.02 Å. In comparison, EGC exhibited a docking score of −3.49 kcal/mol and interacted with *ARG112*, *VAL110*, and *ASP94* through multiple contacts ranging from approximately 3.37 Å to 4.70 Å, suggesting relatively weaker but stable interactions. Comparison with co-crystallized ligands indicated that several interactions of RVG and EGC were comparable and supportive of native ligand binding, further validating their binding potential (Table 6). Among these targets, *MAPK1* shows the most favorable docking score for both RVG and EGC, exhibiting the lowest docking energies and extensive interactions with key active-site residues. Therefore, *MAPK1* is selected for subsequent molecular dynamics (MD) simulations to further investigate the stability and dynamic behavior of the protein–ligand complexes. The 2D and 3D interaction profiles (Figures 7 and 8) further show the binding conformations and key interacting residues, highlighting the ability of RVG and EGC to effectively target multiple AD-related targets.

Table 4. Analysis of RVG and EGC binding affinities in comparison with co-crystal ligands.

Targets	PDB	Docking Energy (kcal/mol)	Interacting Residues	RMSD Range (Å)	Validation Method
NFKB1	8TQD	−5.02	GLU 62, ARG 56, ALA 244, ARG 58, LYS 243	1.10 Å	Redocking of the co-crystallized ligand
MAPK1	1TVO	−7.01	ASP 111, LYS 151, ASP 167, LYS 164	1.24 Å	
STAT1	1YVL	−5.63	GLU 618, ALA 630, MET 654	0.82 Å	
PRKACA	2GU8	−8.22	GLU 170, LYS 168, ASP 166, THR 51, LYS 168, GLU 127	0.60 Å	
GRB2	7MPH	−4.90	ARG 112, VAL 110, ASP 94	1.50 Å	

Table 5. Binding scores of RVG and EGC toward AD target proteins.

Target	PDB	Ligand Name	Docking Energy (kcal/mol)	Binding Residues
NFKB1	8TQD	RIV	−7.94	LYS 243, ALA 244, TYR 59
		EPI	−6.79	GLU 62, ARG 56, ALA 244, ARG 58, PHE 55, GLY 54
MAPK1	1TVO	RIV	−8.63	LYS 164, ASP 162, GLN 132, ARG 135, ARG 79, HIE 80, GLU 81, ASN 82, ILE 83, ILE 84, GLY 85
		EPI	−7.32	ASP 111, LYS 151, ASP 167, ASN 154, SER 153, ASP 149, ARG 67, ILE 31, GLY 32, GLU 33, GLY 34, TYR 36, VAL 39, LYS 54
STAT1	1YVL	RIV	−5.28	MET 654, ALA 656, ALA 655, VAL 653, GLU 618, TRP 616, HIE 629
		EPI	−6.61	GLU 618, ALA 630, TRP 616, HIE 629, VAL 631, GLU 632, ALA 656, ALA 655, MET 654, VAL 653
PRKACA	2GU8	RIV	−4.81	LYS 168, GLU 127, ASP 166, GLU170, ASN 171, TYR 330, PHE 187, ASP 184, PHE 129, SER 53, GLY 52, THR 51, GLY 50, LEU 49
		EPI	−4.61	GLU 170, LYS 168, ASP 166, THR 51, GLY 52, SER 53, THR 201, PHE 187, ASP 184, ASN 171
GRB2	7MPH	RIV	−3.74	ASP 94, SER 96, LYS 109, LEU 111, ARG 112
		EPI	−3.49	ARG 112, VAL 110, ASP 94, LEU 111, LYS 109, SER 96, PHE 95, SER 88, ARG 86

Table 6. Protein-ligand interaction patterns and bond lengths of RIV and EPI.

Target	PDB	Ligand Name	Type of Interaction	Binding Residue	Ligand Atom (or) Ring	Predicted Distance (Å)
NFKB1	8TQD	RIV	Conventional H-bond Interaction	LYS 243	H atom	5.68
		EPI		GLU 62, ARG 56, ALA 244,	H atom	4.42
					O atom	4.29
					H atom	4.47
MAPK1	1TVO	RIV	Conventional H-bond	LYS 164	Benzene ring	5.96
					O atom	5.36
		EPI		ASP 111, LYS 151, ASP 167	H atom	4.46
					H atom	5.79
					H atom	4.37
STAT1	1YVL	RIV	Conventional H-bond Interaction	MET 654	H atom	5.42
					O atom	4.46
		EPI		GLU 618, ALA 630	H atom	4.42
					H atom	4.08
PRKACA	2GU8	RIV	Conventional H-bond Interaction	GLU 127 LYS 168	H atom	5.66
					O atom	6.04
		EPI		LYS 168, ASP 166, GLU170	O atom	5.21
					H atom	4.53
					H atom	4.13
GRB2	7MPH	RIV	Conventional H-bond	ASP 94	H atom	4.02
		EPI		ARG 112, VAL 110, ASP 94	H atom	3.43
					H atom	4.70
					H atom	3.37

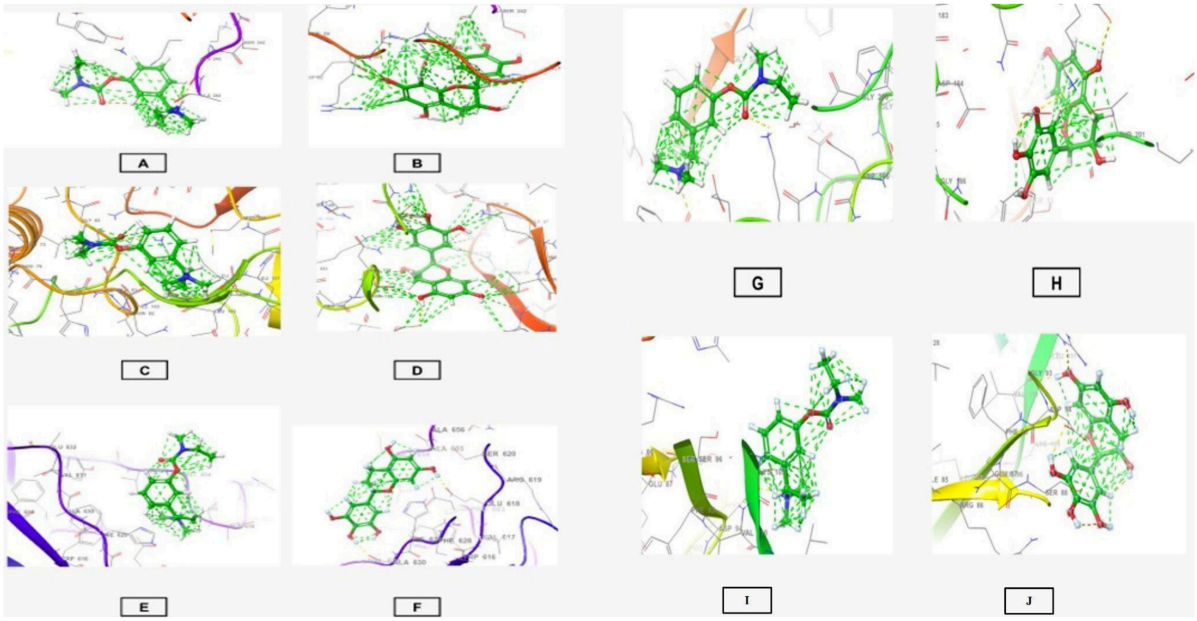

Figure 7. 3D protein-ligand interaction poses of RVG and EGC with key AD targets. (**A**) (NFKB1:RVG), (**B**) (NFKB1:EGC), (**C**) (MAPK1:RVG), (**D**) (MAPK1:EGC), (**E**) (STAT1:RVG), (**F**) (STAT1:EGC), (**G**) (PRKACA:RVG), (**H**) (PRKACA:EGC), (**I**) (GRB2:RVG), (**J**) (GRB2:EGC). Ligands are represented as orange stick structures, and proteins are represented in ribbon form. Green dotted lines represent hydrogen-bond interactions with active position residues.

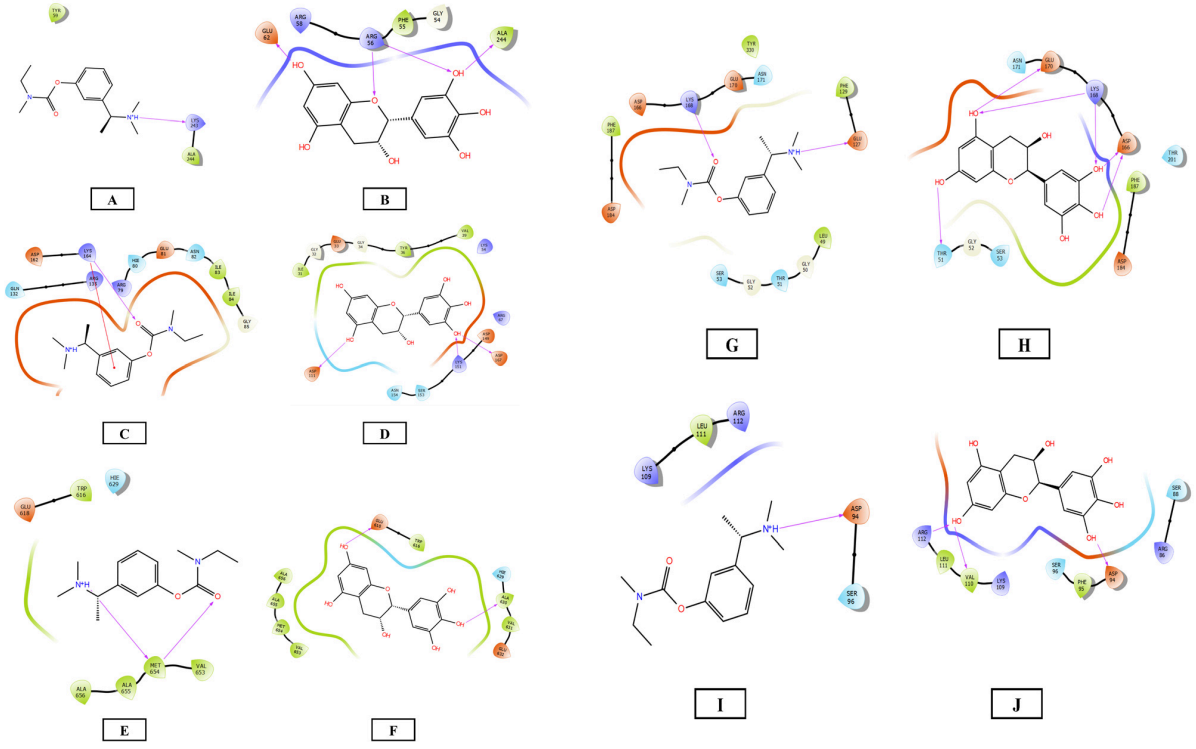

Figure 8. 2D protein-ligand interaction poses of RVG and EGC with key AD targets. (**A**) (NFKB1:RVG), (**B**) (NFKB1:EGC), (**C**) (MAPK1:RVG), (**D**) (MAPK1:EGC), (**E**) (STAT1:RVG), (**F**) (STAT1:EGC), (**G**) (PRKACA:RVG), (**H**) (PRKACA:EGC), (**I**) (GRB2:RVG), (**J**) (GRB2:EGC). Colored spheres show amino acid residues based on their physicochemical characteristics: green indicates hydrophobicity, blue indicates positive charge, red indicates negative charge, and cyan indicates polar residues. Hydrogen bonds formed with backbone or side-chain residues are shown by pink arrows, while green lines correspond to π–cation contacts.

5. Molecular Dynamics (MD) Studies

5.1. RMSD-Based Stability Assessment

The structural stability and conformational changes in RVG and EGC complexes during the 200 ns MD simulation are analyzed using RMSD analysis. As represented in (Figure 9A), the RVG-MAPK1 ligand-protein complex undergoes an initial equilibration phase within the first 30–40 ns, followed by stabilization of the (Cα RMSD) protein backbone around ~2.4–2.8 Å. The ligand RMSD shows a gradual increase, particularly after ~130 ns, reaching ~2.5–3.0 Å, which suggests adaptive conformational flexibility and dynamic repositioning within the binding pocket. This indicates improved accommodation within the active site, supporting sustained interactions over the simulation. In contrast, the EGC-MAPK1 complex (Figure 9B) exhibits rapid equilibration within the first 20 ns, with both protein and ligand RMSD stabilizing consistently around ~2.0–2.5 Å. The ligand RMSD remains steady with minimal fluctuations, indicating stable binding and strong retention within the active site throughout the simulation period. However, both complexes showed favorable stability profiles, with EGC contributing structural rigidity and consistent binding, while RVG exhibits adaptive flexibility that may enhance binding site accommodation.

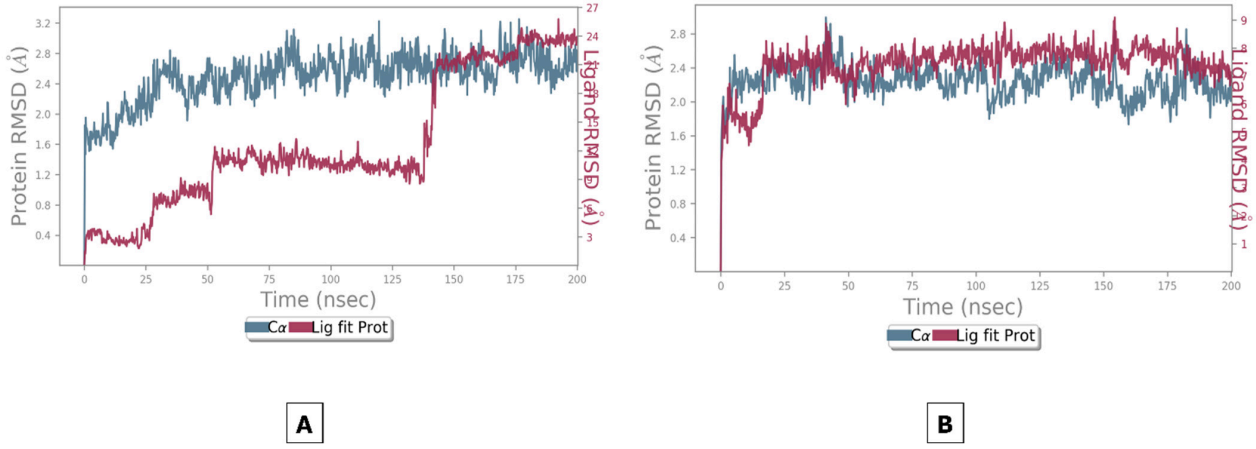

Figure 9. RMSD profiles of Rivastigmine and Epigallocatechin complexes during molecular dynamics simulation. (**A**) Represents the RVG-MAPK1complex, showing gradual stabilization with significant ligand fluctuations at later simulation time, indicating conformational rearrangement within the binding pocket. (**B**) Represents the EGC-MAPK1 complex, indicating stable protein and ligand RMSD with minimal deviations, suggesting strong and consistent binding. The blue line indicates the protein backbone (Cα)-RMSD, and the red line indicates ligand-RMSD.

5.2. RMSF-Based Flexibility Assessment

The flexibility of individual protein residues in complex with RVG and EGC is analyzed by RMSF analysis. As represented in (Figure 10A), the RVG-MAPK1complex indicates relatively stable residue fluctuations, with moderate peaks exhibited in loop regions, particularly toward the terminal residues (~300–330). These localized fluctuations indicate flexible regions that may facilitate conformational adaptability without disrupting the overall structural integrity. Importantly, the binding site residues exhibit relatively low RMSF values (<2.0 Å), suggesting that RVG maintains stable interactions within the active site while allowing adaptive flexibility in peripheral regions. In contrast, the EGC-MAPK1complex (Figure 10B) exhibits comparatively lower residue fluctuations across the majority of the protein structure. Minor peaks are observed in loop regions, consistent with natural protein dynamics; however, the binding site residues remain highly stable with RMSF values predominantly below ~1.5–2.0 Å. This indicates strong stabilization of the active site and effective retention of EGC throughout the simulation.

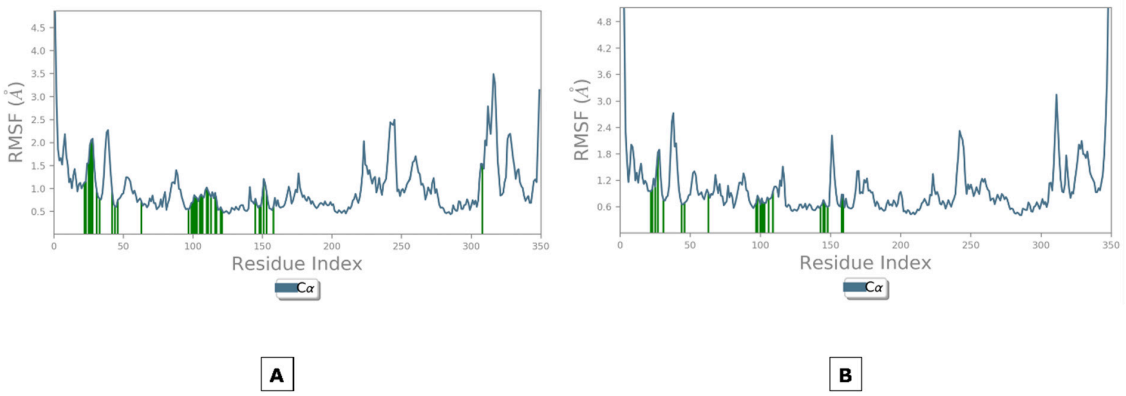

Figure 10. RMSF profiles of Rivastigmine and Epigallocatechin complexes during molecular dynamics simulation. (**A**) RVG-MAPK1 complex. (**B**) EGC-MAPK1 complex. The plot represents residue-wise RMSF (Å) of the protein backbone (Cα) over the simulation period.

5.3. Protein–Ligand Interaction Analysis

Protein-ligand interaction analysis is used to find out how the protein complexes (RVG, EGC) have key contacts during the MD simulation. The complex of RVG-MAPK1 shows a strong interaction with the presence of those key residues that form the hydrogen bond network, which is responsible for the maintenance of ligand arrangement in the target binding site, as shown in (Figure 11A). No matter how much time the simulation runs for, hydrogen-bond interactions are consistently seen, which shows continued binding stability. Hydrophobic contacts from the residues THY30, HIS125 and TRP also stabilize the ligand positioned within the hydrophobic pocket of the active binding site. Electrostatic complementarity is improved with the presence of charged residues, such as GLU109 and ASP124. Moreover, many water-mediated HIS125, LEU156, TYR128, and other residue-by-residue contacts are seen, among others, which allow indirect contacts and overall conformational stability. However, the other EGC-MAPK1 complex (Figure 11B) suggests a large and very stable interaction with the binding residues ILE31, GLU33, GLY71, GLN105 and MET108, which remain stable throughout the simulation. Several hydrogen bonds (usually 3–5) imply strong binding in the active pocket because of the presence of several hydrogen bonds. Further contacts with ligands are hydrophobic contacts from VAL39, LEU1560, and ALA52. Water bridges are also clearly seen, including residues LYS54 and MET108, which increase the stability of the interaction and the ability to adapt its dynamics with the help of water.

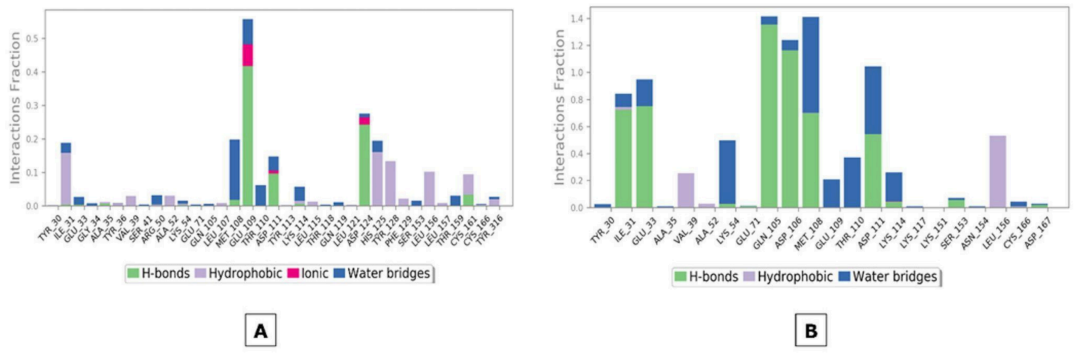

Figure 11. Protein-ligand interaction profiles of RVG and EGC complexes during MD simulation. (**A**) RVG-MAPK1 complex. (**B**) EGC-MAPK1 complex. The bars represent interaction fractions of hydrophobic contacts, hydrogen bonds, water bridges, and ionic interactions, formed with individual residues over the simulation period.

5.4. Ligand-Protein Contact Analysis

The key active residues in the active binding region that contribute to the stability of RVG and EGC are identified through the ligand-protein contact analysis. The complex of RVG-MAPK1 shows a significant ionic bond between the protonated amine group of the ligand and GLU109, which could be a key electrostatic interaction for the stabilization of the binding pocket. Moreover, the orientation and accommodation of the polar carbamate group are further supported by the surrounding polar contacts. These interactions guarantee the stability of RVG, with very little alteration of the RVG structure and also effective positioning in the active region. The EGC-MAPK1 complex (Figure 12) has a wide hydrogen-bonding interaction network, including several residues, such as GLU33, LYS54, GLN59, ASP106, ASP111, MET108, LEU156 and ILE31. The 'hydroxyl' groups on the ligand allow multiple and strong hydrogen-bond interactions and often these interactions are direct or are mediated by other water molecules, making ligand binding more stable.

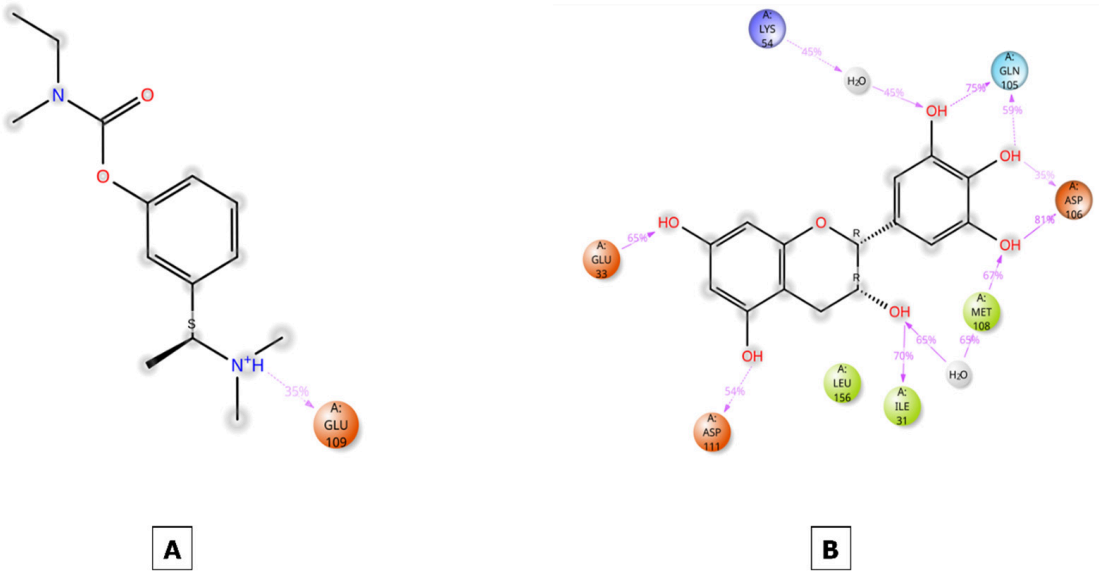

Figure 12. Ligand-protein interaction diagrams of Rivastigmine and Epigallocatechin within the binding site. (**A**) RVG protein complex. (**B**) EGC protein complex. Dashed lines represent hydrogen bonds and water-mediated interactions, while colored residues indicate interacting amino acids within the binding pocket.

6. Synergy Analysis by CompuSyn

The cytotoxic effects of RVG, EGC, and their fixed-ratio combinations (1:1, 1:2, and 2:1) were evaluated by MTT assay, and the corresponding median-effect parameters were determined using CompuSyn analysis (Figures 13 and S1). Individual treatments exhibited median-effect doses (Dm) of 66.59 μM and 63.57 μM for RVG and EGC, respectively. Among the combination treatments, the RVG (2:1) ratio showed the lowest Dm value (23.46 μM), followed by the 1:1 ratio (38.22 μM), whereas the 1:2 ratio exhibited a Dm of 58.83 μM. The reduced Dm values observed for the combination treatments compared with the individual compounds indicate enhanced cytotoxic potency.

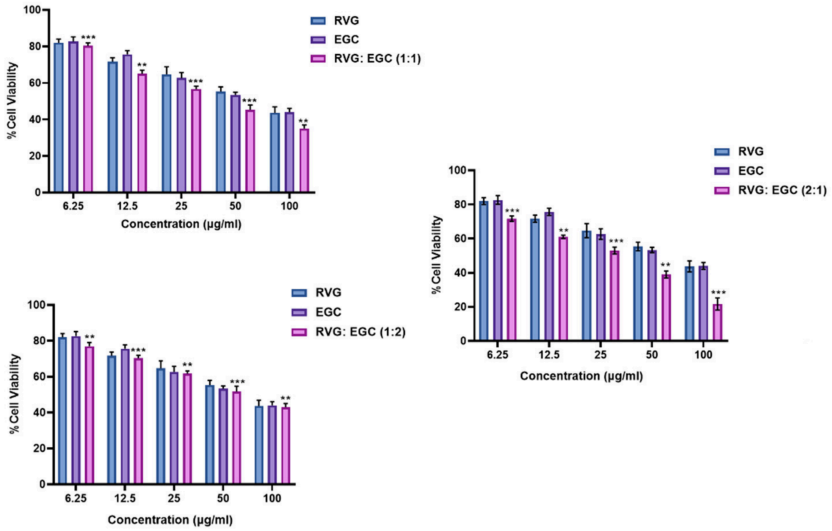

Figure 13. Cytotoxic effects of RVG, EGC, and their combinations. RVG:EGC (1:1), RVG:EGC (1:2), and RVG:EGC (2:1). Cells were treated with increasing concentrations (6.25–100 µg/mL), and the MTT assay determines cell viability. The cytotoxic effects of the combination treatments were compared with those of the respective individual compounds, RVG and EGC, to evaluate the impact of different combination ratios on cell viability. Data are presented as mean ± SE from three independent experiments ($n = 3$). Statistical analysis was performed using two-way ANOVA followed by Tukey's post hoc test. ** $p < 0.01$ and *** $p < 0.001$ compared with the respective individual drug-treated groups.

6.1. Median-Effect Plot Analysis

Median-effect plots generated using CompuSyn software are used to characterize the dose-effect relationships of RVG, EGC, and their fixed-ratio combinations, as shown in Figure 14. Figure 14A shows the median-effect plots of the individual compounds, RVG and EGC, both exhibiting linear dose–response relationships. Figure 14B presents the median-effect plots for the three fixed-ratio combinations of RVG:EGC (1:1), RVG:EGC (1:2), and RVG:EGC (2:1). Among the combinations, the RVG:EGC (2:1) ratio showed the most pronounced leftward shift, followed by the 1:1 ratio, indicating greater effects at lower concentrations relative to the other treatment groups.

The median-effect dose (Dm), slope (m), and correlation coefficient (r) values obtained from CompuSyn analysis are summarized in Table 7. The individual treatments exhibited Dm values of 66.59 µM for RVG and 63.57 µM for EGC. All combination groups showed reduced Dm values compared with the individual compounds, with the RVG: EGC (2:1) ratio exhibiting the lowest Dm value (23.46 µM), followed by the 1:1 (38.22 µM) and 1:2 (58.83 µM) ratios. The slope (m) values ranged from −0.5457 to −0.7704, and all treatments showed high correlation coefficients (r = −0.9778 to −0.9895), indicating a strong linear fit of the dose-effect data. These findings supported the suitability of the experimental data for subsequent combination index (CI) analysis.

Table 7. Median-effect plot parameters.

Treatment	Median-Effect Dose, Dm (µM)	Slope, m	Correlation Coefficient, r
RVG	66.5927	−0.6233	−0.9800
EGC	63.5688	−0.6709	−0.9840
RVG:EGC (1:1)	38.2236	−0.7019	−0.9843
RVG:EGC (1:2)	58.8297	−0.5457	−0.9895
RVG:EGC (2:1)	23.4602	−0.7704	−0.9778

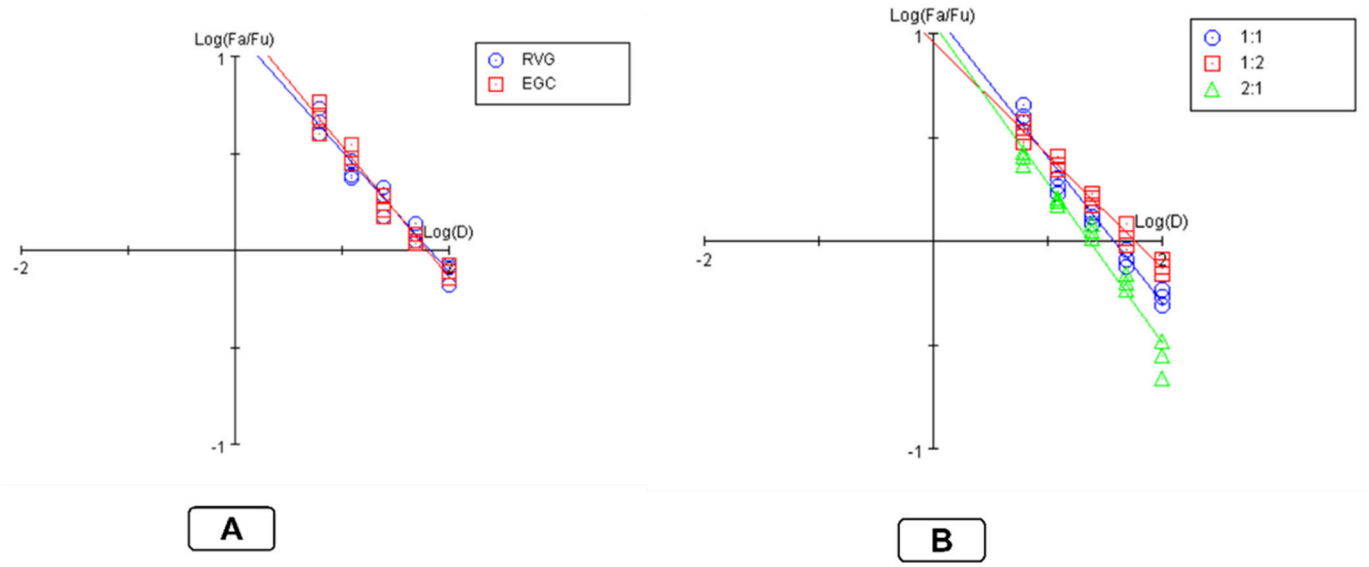

Figure 14. Median-effect plots for the dose–effect relationship. (**A**) Represents the median-effect plots of the individual compounds, RVG and EGC. (**B**) Shows the median-effect plots for the fixed-ratio combinations of RVG and EGC: blue line (1:1), red line (1:2), and green line (2:1). The combination curves exhibit a leftward shift relative to the monotherapy curves, indicating increased effects at lower concentrations. The plots were generated using CompuSyn software based on the median-effect principle to characterize the dose–response relationships of individual compounds and their combinations.

6.2. Combination Interaction and Dose Reduction Analysis

The Fa-CI plot depicts the relationship between the fraction affected (Fa) and the corresponding combination index (CI) values for the RVG fixed-ratio combinations (1:1, 1:2, and 2:1), as shown in Figure 15A. All combinations exhibited CI values below 1 at ED50, ED75, and ED90, indicating synergistic interactions (Table 8). Among the evaluated combinations, RVG (1:1) at ED50 (CI = 0.58764) and RVG (1:2) at ED75 (CI = 0.65301) were selected for subsequent studies. The 1:1 combination at ED50 (50% inhibition) is chosen to represent a balanced high-dose regimen with equal contributions from both compounds, whereas the 1:2 combination at ED75 (75% inhibition) is selected as a low-dose regimen capable of achieving a higher effect level with reduced drug exposure. These combinations were therefore considered suitable for evaluating the biological effects of RVG and EGC under distinct synergistic dosing conditions.

Table 8. Combination index and dose reduction parameters.

Fa (Effect Level)	Combination	CI Value	RVG Dose (μM)	EGC Dose (μM)
0.50 (ED50)	1:1	0.58764	19.1118	19.1118
	1:2	0.91144	19.6099	39.2198
	2:1	0.35788	15.6402	7.82008
0.75 (ED75)	1:1	0.67289	3.99544	3.99544
	1:2	0.65301	2.61924	5.23848
	2:1	0.48085	3.75766	1.87883
0.90 (ED90)	1:1	0.77351	0.83527	0.83527
	1:2	0.46953	0.34984	0.69969
	2:1	0.64825	0.90281	0.45140

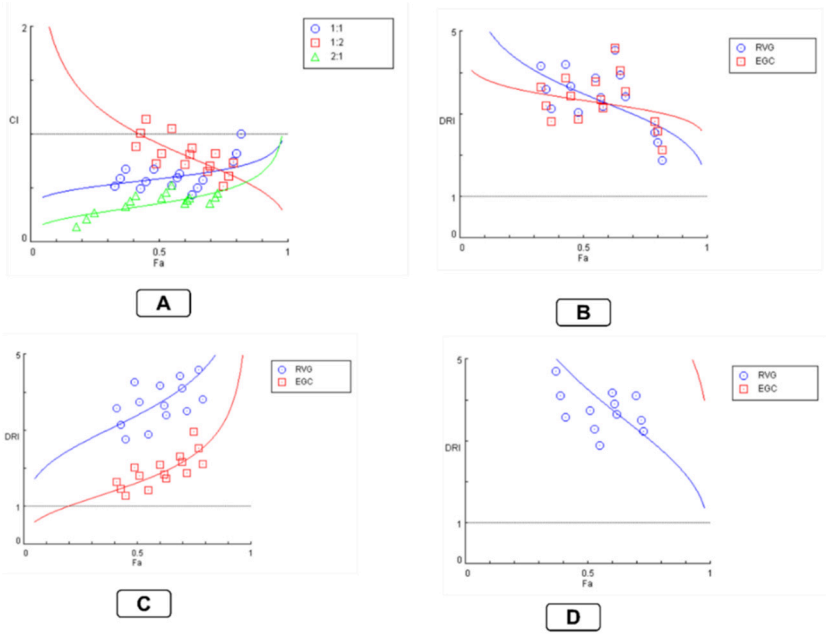

Figure 15. CompuSyn-generated plots showing (**A**) Fa-CI analysis of RVG and EGC combinations at fixed ratios (1:1, 1:2, and 2:1). (**B**–**D**) Dose reduction index (DRI) plots showing the dose reduction potential of RVG and EGC across the tested combinations: (**B**) 1:1, (**C**) 1:2, and (**D**) 2:1.

The dose reduction index (DRI) plots generated by CompuSyn are shown in Figure 15B–D. Figure 15B shows the DRI profile for the 1:1 combination, in that both RVG and EGC exhibited dose reduction across the examined Fa range. Figure 15C represents the DRI profile of the 1:2 combination, where RVG showed comparatively higher DRI values than EGC. Figure 15D depicts the DRI profile for the 2:1 combination, showing dose reduction for both compounds throughout the tested effect range. These indicate the potential for reducing the doses of RVG and EGC while maintaining the desired cytotoxic effect.

7. Discussion

AD is a progressive neurodegenerative disease characterized by cognitive deterioration, impaired synaptic function, and neuronal loss. The pathologies of AD, such as tau hyperphosphorylation, amyloid-β aggregation, mitochondrial dysfunction, and chronic neuroinflammation, are regulated by highly interconnected molecular pathways rather than a single causative mechanism. This complexity has limited the success of conventional single-target therapies, highlighting the urgent need for multi-target therapeutic strategies for modulating multiple pathological processes simultaneously. One of the central mediating factors of AD progression is chronic neuroinflammation, primarily driven by microglial activation and dysregulated immune signaling. Persistent activation of inflammatory pathways leads to excessive production of cytokines, oxidative stress, and neuronal damage. Key signaling molecules such as NF-κB and *STAT1* act as transcriptional regulators of inflammatory gene expression, linking extracellular stress signals to intracellular responses. Dysregulation of these pathways contributes to sustained inflammation and neuronal dysfunction, suggesting that targeting upstream signaling networks shows a more effective therapeutic approach. Therefore, targeting MAPK1/ERK within the PD-1/PD-L1 signaling context represents a dual-action therapeutic strategy that inhibits kinase-driven pathological processes while modulating neuroimmune responses [30,31].

Unlike previous studies that primarily focused on the individual neuroprotective properties of RVG or catechin-derived compounds, the present work highlights a relatively unexplored convergence between immune checkpoint-associated signaling and kinase-

mediated neuroinflammatory pathways. The identification of *MAPK1* as a major hub gene together with enrichment of the PD-1/PD-L1 signaling pathway suggests that neuroimmune regulation and intracellular stress signaling may cooperatively contribute to AD progression.

Among the critical intracellular signaling pathways, the MAPK/ERK pathway plays a significant role in regulating neuronal survival, stress responses, and synaptic plasticity. The RAS-RAF-MEK-ERK pathway integrates extracellular stimuli and modulates downstream transcription factors such as AP-1 and NF-κB. Under physiological conditions, ERK activation supports learning and memory processes; however, in AD, aberrant and sustained ERK activation is strongly associated with tau hyperphosphorylation, synaptic impairment, and neuronal apoptosis. Additionally, ERK signaling interacts with other kinase-driven pathways, including *CDKs* and *PRKACA*, further enhancing pathological phosphorylation. Therefore, modulation of ERK signaling represents a significant therapeutic strategy to restore cellular homeostasis and prevent neurodegenerative progression.

A particularly important mechanism emerging from this study is the interplay between the PD-1/PD-L1 immune checkpoint signaling pathway and MAPK/ERK (MAPK1) signaling, which provides a novel link between neuroimmune regulation and intracellular kinase-driven neurodegeneration in Alzheimer's disease. The PD-1/PD-L1 signaling pathway is a significant regulator of immune homeostasis, functioning to inhibit excessive T-cell stimulation and maintain immune tolerance. In the central nervous system, this pathway is increasingly associated with the modulation of microglial activity and neuroinflammatory responses. Dysregulation of PD-1/PD-L1 signaling can lead to impaired clearance of amyloid-β and sustained inflammatory activation, thereby contributing to disease progression. Mechanistically, PD-L1 expression is tightly regulated by upstream signaling cascades, including receptor tyrosine kinase activation and cytokine-mediated pathways, that converge on intracellular signaling networks such as PI3K/AKT and the MAPK cascade [25]. The MAPK/ERK pathway plays an important role in transducing extracellular signals into transcriptional responses through activation of downstream effectors such as AP-1 and NF-κB. Aberrant activation of ERK has been strongly implicated in tau hyperphosphorylation, synaptic dysfunction, and neuronal stress responses in AD. Importantly, activation of ERK signaling can enhance PD-L1 expression, thereby establishing a feedback loop that links intracellular stress signaling with immune checkpoint regulation. This crosstalk suggests that modulation of *MAPK1* not only influences neuronal survival pathways but also indirectly regulates immune signaling dynamics within the brain. Therefore, targeting ERK within the PD-1/PD-L1 signaling context represents a dual-action therapeutic strategy, capable of attenuating kinase-driven pathological processes while simultaneously modulating neuroimmune responses. Such integrated regulation may reduce chronic inflammation, restore immune balance, and limit neurodegenerative progression, highlighting the significance of this pathway as a key mechanistic bridge in Alzheimer's disease pathology [26].

The combined use of RVG and EGC therefore represents a mechanistically complementary strategy, where RVG primarily contributes to neurotransmitter balance and immune modulation, while EGC provides broad-spectrum regulation of oxidative stress, kinase signaling, and protein aggregation pathways. This dual mechanism complies with the principles of network pharmacology, where simultaneous modulation of interconnected pathways leads to enhanced therapeutic efficacy compared to single-target interventions. Importantly, the connections between MAPK/ERK signaling and PD-1/PD-L1-mediated immune regulation provide a novel mechanistic basis for this combination. By influencing upstream signaling nodes and immune checkpoints, the combined modulation of these pathways may reduce neuroinflammation, limit abnormal phosphorylation events, and im-

prove neuronal survival. Additionally, the regulation of downstream transcription factors, including NF-κB, further supports the suppression of inflammatory gene expression, contributing to a neuroprotective environment. Further experimental validation and clinical investigations are necessary to validate these findings and assess their therapeutic potential in AD management.

The proposed mechanisms are further supported by previously reported in vitro studies. RVG has been shown to improve cholinergic neurotransmission and protect neuronal cells against neurotoxic injury [32]. In contrast, catechin-derived polyphenols, including EGC, showed antioxidant, anti-inflammatory, and anti-amyloid activities through modulation of MAPK/ERK signaling and inflammatory mediators in neuronal and glial cell models [33]. These experimental observations are consistent with the computational predictions of the present study and provide biological support for the proposed *MAPK1*-associated mechanisms. However, direct validation of the RVG-EGC combination remains necessary (Figure 16).

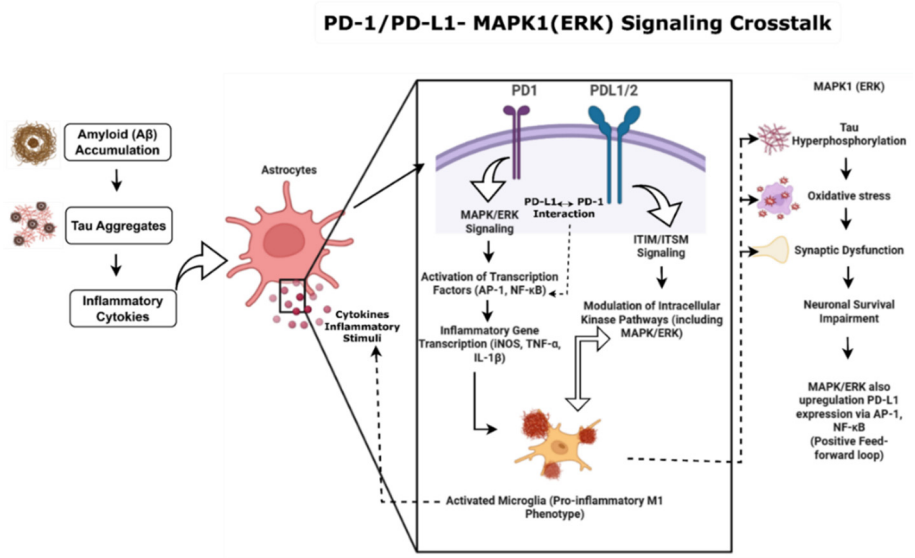

Figure 16. PD-1/PD-L1-MAPK1 (ERK) signaling crosstalk in AD. Amyloid-β (Aβ) accumulation, tau aggregation, and inflammatory cytokines activate astrocytes and microglia, promoting PD-1/PD-L1 signaling and *MAPK1* (ERK) pathway activation. This crosstalk enhances AP-1/NF-κB-mediated inflammatory gene expression, leading to increased production of pro-inflammatory mediators, microglial activation, tau hyperphosphorylation, oxidative stress, synaptic dysfunction, and neuronal survival impairment. *MAPK1* (ERK) signaling may also upregulate PD-L1 expression, forming a positive feed-forward loop that sustains neuroinflammation and contributes to Alzheimer's disease progression.

The synergistic interaction between RVG and EGC is further validated using the Chou-Talalay method, with all fixed-ratio combinations exhibiting CI values below 1. Based on the degree of synergism and dose requirements, the RVG: EGC (1:1) combination at ED50 (CI = 0.58764) and the RVG: EGC (1:2) combination at ED75 (CI = 0.65301) were selected for subsequent studies to represent balanced high-dose and effective low-dose regimens, respectively. This dose optimization strategy highlights the advantage of combining RVG and EGC, enabling enhanced efficacy at reduced concentrations and providing a rational basis for their development as a multi-target therapeutic approach for AD. To date, no published studies specifically evaluated the pharmacokinetic or pharmacodynamic interactions between RVG and EGC. Although catechin-containing preparations are reported to influence the activity of certain drug-metabolizing enzymes and transporters, the clinical relevance of these interactions with RVG remains unclear. Therefore, pharmacokinetic and

safety studies are warranted to evaluate the potential herb-drug interactions of the RVG-EGC combination. In addition, protein-level in vitro and preclinical studies are required to validate these findings and assess their therapeutic potential in AD management.

8. Study Limitations and Future Perspectives

The findings are currently limited to computational predictions, highlighting the need for experimental confirmation of the RVG-EGC therapeutic effects in AD. Future studies will include in vitro evaluation using neuronal cell lines (e.g., SH-SY5Y, PC12) to assess neuroprotection, anti-inflammatory effects, and modulation of amyloid-β and tau pathology. In vivo validation will be performed in transgenic AD models to evaluate cognitive function and disease progression. Pharmacokinetic studies will determine parameters such as half-life ($t_1/_2$), Cmax, AUC, and BBB, while biodistribution analysis will assess brain targeting and systemic safety. Mechanistic validation will be carried out using Western blotting and RT-qPCR to examine key pathways, particularly MAPK/ERK and PD-1/PD-L1 signaling (*MAPK1*, NF-κB, *STAT1*). Functional assays, including ROS, apoptosis, and mitochondrial activity, will further clarify the therapeutic effects. These studies will support the translational potential of the RVG-EGC combination as a multi-target strategy for Alzheimer's disease.

9. Conclusions

The present study provides an integrated computational approach and quantitative synergy assessment supporting the potential of the RVG-EGC combination as a multi-target therapeutic strategy for AD. Network pharmacology, molecular docking, molecular dynamics simulations, and Chou-Talalay combination analysis suggest that RVG and EGC may exert interconnected mechanisms through *MAPK1*-associated signaling networks while showing synergistic interactions at selected dose combinations. These findings provide a computational rationale for understanding the potential involvement of neuroimmune regulation and kinase-mediated signaling in the proposed therapeutic effects of the RVG-EGC combination. KEGG enrichment analysis further indicated the involvement of genes associated with the PD-1/PD-L1 signaling pathway, suggesting a potential link between neuroimmune regulation and kinase-mediated signaling processes in the proposed therapeutic effects of the RVG-EGC combination. However, further in vitro and in vivo investigations are required to validate these predicted molecular mechanisms and determine their biological significance and therapeutic potential for AD.

Supplementary Materials: The following supporting information can be downloaded at: https://www.mdpi.com/article/10.3390/scipharm94030057/s1, Figure S1: Microscopic images of SH-SY5Y cells following treatment with rivastigmine at different concentrations (6.25, 12.5, 25, 50, and 100 μg/mL); Figure S2: Microscopic images of SH-SY5Y cells following treatment with epigallocatechin at different concentrations (6.25, 12.5, 25, 50, and 100 μg/mL); Figure S3: Microscopic images of SH-SY5Y cells following treatment with 1:1 ratio of rivastigmine and epigallocatechin at different concentrations (6.25, 12.5, 25, 50, and 100 μg/mL); Figure S4: Microscopic images of SH-SY5Y cells following treatment with 1:2 ratio of rivastigmine and epigallocatechin at different concentrations (6.25, 12.5, 25, 50, and 100 μg/mL); Figure S5: Microscopic images of SH-SY5Y cells following treatment with 2:1 ratio of rivastigmine and epigallocatechin at different concentrations (6.25, 12.5, 25, 50, and 100 μg/mL); Table S1 Summary of Chou–Talalay combination index (CI) analysis of rivastigmine (RVG) and epigallocatechin (EGC) combinations.

Author Contributions: B.D. Conceptualization, Methodology, Writing—Review and Editing, Writing—original draft, Visualization; M.S.U. Data Curation, Validation, Visualization, Supervision. All authors have read and agreed to the published version of the manuscript.

Funding: The article was prepared without the use of any external funding sources.

Institutional Review Board Statement: Not applicable.

Informed Consent Statement: Not applicable.

Data Availability Statement: This article contains no datasets generated or analyzed during the current study.

Acknowledgments: The authors gratefully acknowledge SRM College of Pharmacy, Faculty of Medical and Health Science, SRMIST, for providing the necessary infrastructure, technical assistance, and academic support that greatly facilitated the successful completion of this research work.

Conflicts of Interest: The authors declare that they have no known competing financial interests or personal relationships that could have appeared to influence the work reported in this paper.

Abbreviations

The following abbreviations are used in this manuscript:

AD	Alzheimer's Disease
RVG	Rivastigmine
EGC	Epigallocatechin
Aβ	Amyloid-beta
BBB	Blood–Brain Barrier
CNS	Central Nervous System
PPI	Protein–Protein Interaction
CTPD	Compound-Target-Pathway-Disease
GO	Gene Ontology
KEGG	Kyoto Encyclopedia of Genes and Genomes
BP	Biological Process
CC	Cellular Component
MF	Molecular Function
MD	Molecular Dynamics
RMSD	Root Mean Square Deviation
RMSF	Root Mean Square Fluctuation
H-bond	Hydrogen Bond
ROS	Reactive Oxygen Species
MAPK	Mitogen-Activated Protein Kinase
ERK	Extracellular Signal-Regulated Kinase
NF-κB	Nuclear Factor kappa B
STAT1	Signal Transducer and Activator of Transcription 1
PI3K	Phosphoinositide 3-Kinase
AKT	Protein Kinase B
PD-1/PD-L1	Programmed Cell Death Protein 1/Programmed Death-Ligand 1

References

1. Lamptey, R.N.L.; Chaulagain, B.; Trivedi, R.; Gothwal, A.; Layek, B.; Singh, J. A Review of the Common Neurodegenerative Disorders: Current Therapeutic Approaches and the Potential Role of Nanotherapeutics. *Int. J. Mol. Sci.* **2022**, *23*, 1851. [CrossRef] [PubMed] [PubMed Central]
2. Gao, W.; Jing, S.; He, C.; Saberi, H.; Sharma, H.S.; Han, F.; Chen, L. Advancements in neurodegenerative diseases: Pathogenesis and novel neurorestorative interventions. *J. Neurorestoratol.* **2025**, *13*, 100176. [CrossRef]
3. Alzheimer's Association. Alzheimer's disease facts and figures. *Alzheimer's Dement.* **2025**, *21*, e70235. [CrossRef] [PubMed Central]
4. Li, M.; Ye, X.; Huang, Z.; Ye, L.; Chen, C. Global burden of Parkinson's disease from 1990 to 2021: A population-based study. *BMJ Open* **2025**, *15*, e095610. [CrossRef] [PubMed] [PubMed Central]
5. Yin, X.; Qiu, Y.; Zhao, C.; Zhou, Z.; Bao, J.; Qian, W. The Role of Amyloid-Beta and Tau in the Early Pathogenesis of Alzheimer's Disease. *Med. Sci. Monit. Int. Med. J. Exp. Clin. Res.* **2021**, *27*, e933084-1–e933084-7. [CrossRef] [PubMed] [PubMed Central]

6. Jahan, I.; Harun-Ur-Rashid, M.; Islam, A.; Sharmin, F.; Al Jaouni, S.K.; Kaki, A.M.; Selim, S. Neuronal plasticity and its role in Alzheimer's disease and Parkinson's disease. *Neural Regen. Res.* **2024**, *21*, 107–125. [CrossRef] [PubMed] [PubMed Central]
7. Miculas, D.C.; Negru, P.A.; Bungau, S.G.; Behl, T.; Hassan, S.S.u.; Tit, D.M. Pharmacotherapy Evolution in Alzheimer's Disease: Current Framework and Relevant Directions. *Cells* **2022**, *12*, 131. [CrossRef] [PubMed] [PubMed Central]
8. Espay, A.J.; Kepp, K.P.; Herrup, K. Lecanemab and Donanemab as Therapies for Alzheimer's Disease: An Illustrated Perspective on the Data. *eNeuro* **2024**, *11*, ENEURO.0319-23.2024. [CrossRef] [PubMed] [PubMed Central]
9. Boxer, A.L.; Sperling, R. Accelerating Alzheimer's therapeutic development: The past and future of clinical trials. *Cell* **2023**, *186*, 4757–4772. [CrossRef] [PubMed]
10. Cummings, J.L.; Osse, A.M.L.; Kinney, J.W.; Cammann, D.; Chen, J. Alzheimer's Disease: Combination Therapies and Clinical Trials for Combination Therapy Development. *CNS Drugs* **2024**, *38*, 613–624. [CrossRef] [PubMed] [PubMed Central]
11. Gopalakrishna, P.K.; Che Mohd Nassir, C.M.N.; Anandan, S.; Hussan, F.; Dandala, K.C.R.; Sura, S.; Jagadeesan, S.; Moklas, M.A.M.; Vishnumukkala, T.; Hein, Z.M. The Immuno-Glial Connectome in Alzheimer's Disease: Integrating Central and Peripheral Inflammatory Networks. *Cell. Mol. Neurobiol.* **2026**, *46*, 31. [CrossRef] [PubMed]
12. Zhang, X.; Huang, S.; Xu, H.; Hu, Y.; Gao, L. Research progress on plant-derived natural compounds regulating the MAPK signaling pathway for the prevention and therapy of Alzheimer's disease. *Front. Pharmacol.* **2025**, *16*, 1666082. Correction in *Front. Pharmacol.* **2025**, *16*, https://doi.org/10.3389/fphar.2025.1710820. [CrossRef] [PubMed]
13. Kannan, K.; Mohan, S. Targeting mTORC1/TGFB1 signaling with a novel Bergapten-Esculetin combination: A computational and experimental approach in idiopathic pulmonary fibrosis. *Mol. Divers.* **2025**, *30*, 4481–4510. [CrossRef] [PubMed]
14. Wu, X.; Zheng, X.; Tang, H.; Zhao, L.; He, C.; Zou, Y.; Song, X.; Li, L.; Yin, Z.; Ye, G. A network pharmacology approach to identify the mechanisms and molecular targets of curcumin against Alzheimer disease. *Medicine* **2022**, *101*, e30194. [CrossRef] [PubMed] [PubMed Central]
15. Gangwal, A.; Ansari, I.; Sawale, J.A.; Ansari, A. Network pharmacology-guided identification and molecular validation of multi-target phytoconstituents from Gmelina arborea against Alzheimer's disease. *Silico Res. Biomed.* **2026**, *2*, 100247. [CrossRef]
16. Li, J.; Zhang, J.; Ke, J.; Ren, Z.; Feng, C. Integrative network pharmacology and machine learning identify potential targets of indole-3-lactic acid in colorectal cancer. *PLoS ONE* **2026**, *21*, e0344478. [CrossRef] [PubMed] [PubMed Central]
17. Hossain, M.A.; Rahman, M.H.; Sultana, H.; Ahsan, A.; Rayhan, S.I.; Hasan, M.I.; Sohel; Somadder, P.D.; Moni, M.A. An integrated in-silico Pharmaco-BioInformatics approaches to identify synergistic effects of COVID-19 to HIV patients. *Comput. Biol. Med.* **2023**, *155*, 106656. [CrossRef] [PubMed] [PubMed Central]
18. Kannan, K.; Pillai, N.P.; Mohan, S.; Kuppusamy, S. Targeting HSP90AA1/mTOR signaling by a novel synergistic bioactive combination of Methotrexate and Vitexin (*Vitex negundo* L.) in lung cancer: An integrated network pharmacology and in-vitro validation approach. *Food Biosci.* **2026**, *79*, 108851. [CrossRef]
19. Harakeh, S.; Niyazi, H.A.; Niyazi, H.A.; Abdalal, S.A.; Mokhtar, J.A.; Almuhayawi, M.S.; Alkuwaity, K.K.; Abujamel, T.S.; Slama, P.; Haque, S. Integrated Network Pharmacology Approach to Evaluate Bioactive Phytochemicals of Acalypha indica and Their Mechanistic Actions to Suppress Target Genes of Tuberculosis. *ACS Omega* **2023**, *9*, 2204–2219. [CrossRef] [PubMed] [PubMed Central]
20. Ye, X.-W.; Wang, H.-L.; Cheng, S.-Q.; Xia, L.-J.; Xu, X.-F.; Li, X.-R. Network Pharmacology-Based Strategy to Investigate the Pharmacologic Mechanisms of Coptidis Rhizoma for the Treatment of Alzheimer's Disease. *Front. Aging Neurosci.* **2022**, *14*, 890046. [CrossRef] [PubMed] [PubMed Central]
21. Gao, X.; Li, S.; Cong, C.; Wang, Y.; Xu, L. A Network Pharmacology Approach to Estimate Potential Targets of the Active Ingredients of Epimedium for Alleviating Mild Cognitive Impairment and Treating Alzheimer's Disease. *Evid.-Based Complement. Altern. Med. ECAM* **2021**, *2021*, 2302680. [CrossRef] [PubMed] [PubMed Central]
22. Patil, N.; Dhariwal, R.; Mohammed, A.; Wei, L.S.; Jain, M. Network pharmacology-based approach to elucidate the pharmacologic mechanisms of natural compounds from *Dictyostelium discoideum* for Alzheimer's disease treatment. *Heliyon* **2024**, *10*, e28852. [CrossRef] [PubMed]
23. Shri, S.R.; Nayak, Y.; Ranganath Pai, S. Molecular docking studies and molecular dynamic simulation analysis: To identify novel ATP-competitive inhibition of Glycogen synthase kinase-3β for Alzheimer's disease. *F1000Research* **2025**, *13*, 773. [CrossRef] [PubMed] [PubMed Central]
24. Vijayakumar, S.; Manogar, P.; Prabhu, S.; Sanjeevkumar Singh, R.A. Novel ligand-based docking; molecular dynamic simulations; and absorption, distribution, metabolism, and excretion approach to analyzing potential acetylcholinesterase inhibitors for Alzheimer's disease. *J. Pharm. Anal.* **2018**, *8*, 413–420. [CrossRef] [PubMed]
25. Mazri, R.; Ouassaf, M.; Zekri, A.; Khan, S.U.; Rengasamy, K.R.R.; Alhatlani, B.Y. In Silico Network Pharmacology, Molecular Docking, and Molecular Dynamics Analysis of Rosemary-Derived Compounds as Potential HSP90 Inhibitors for Cancer Therapy. *Curr. Issues Mol. Biol.* **2025**, *47*, 860. [CrossRef] [PubMed] [PubMed Central]

26. Vikhar Danish Ahmad, A.; Khan, S.W.; Ali, S.A.; Yasar, Q. Network pharmacology combined with molecular docking and experimental verification to elucidate the effect of flavan-3-ols and aromatic resin on anxiety. *Sci. Rep.* **2024**, *14*, 9799. [CrossRef] [PubMed]
27. Chand, J.; Jupudi, S.; Ahmad, S.F.; Emran, T.B.; Subramanian, G. Therapeutic mechanistic study of novel indole derivatives as SIRTUIN3 modulators in Parkinson's disease with in vitro evaluation. *Sci. Rep.* **2025**, *15*, 15196. [CrossRef] [PubMed] [PubMed Central]
28. Banerjee, V.; Sharda, N.; Huse, J.; Singh, D.; Sokolov, D.; Czinn, S.J.; Blanchard, T.G.; Banerjee, A. Synergistic potential of dual andrographolide and melatonin targeting of metastatic colon cancer cells: Using the Chou-Talalay combination index method. *Eur. J. Pharmacol.* **2021**, *897*, 173919. [CrossRef] [PubMed]
29. Chou, T.C. Drug Combination Studies and Their Synergy Quantification Using the Chou-Talalay Method. *Cancer Res.* **2010**, *70*, 440–446. [CrossRef] [PubMed]
30. Han, Y.; Liu, D.; Li, L. PD-1/PD-L1 pathway: Current researches in cancer. *Am. J. Cancer Res.* **2020**, *10*, 727–742. [PubMed] [PubMed Central]
31. Moadab, A.; Khorramdelazad, H.; Javar, M.T.A.; Nejad, M.S.M.; Mirzaie, S.; Hatami, S.; Mahdavi, N.; Ghaffari, S.; Yazdian, F.A. Unmasking a Paradox: Roles of the PD-1/PD-L1 Axis in Alzheimer's Disease-Associated Neuroinflammation. *J. Neuroimmune Pharmacol.* **2025**, *20*, 46. [CrossRef] [PubMed]
32. Siddique, Y.H.; Naz, F.; Rahul; Varshney, H. Comparative study of rivastigmine and galantamine on the transgenic Drosophila model of Alzheimer's disease. *Curr. Res. Pharmacol. Drug Discov.* **2022**, *3*, 100120. [CrossRef] [PubMed]
33. Li, S.; Wang, Z.; Liu, G.; Chen, M. Neurodegenerative diseases and catechins: (−)-epigallocatechin-3-gallate is a modulator of chronic neuroinflammation and oxidative stress. *Front. Nutr.* **2024**, *11*, 1425839. [CrossRef] [PubMed] [PubMed Central]